AN ABSTRACT OF THE THESIS OF

Abdullah Al-Kahtani for the degree of Master of Science in Chemistry presented on December 2, 1991

Title: High Resolution Spectroscopy Of BeB_2H_8 and C_2H_6

Abstract approved: Redacted for Privacy

The utility of high resolution spectroscopy has been investigated for two molecules. First, a prediction of the spectra of BeB_2H_8 was made from detailed theoretical calculations based on proposed structures by Stanton et al. The rotational constants, as well as the nuclear spin statistical weights, were calculated for the four most probable conformers (D_{2d}, D_{3d}, C_s, and C_{3v}). The results showed that the molecular structure of BeB_2H_8 would be difficult to establish by just considering the rotational constants of the four different isomers in a spectral study. However, the line intensity alternation predicted for the different K values showed that it would be possible to distinguish structures with a three-fold symmetry axis (D_{3d} or C_{3v}) from one with two-fold symmetry axis (D_{2d}). Simulation of the different kinds of spectra showed that a high resolution FTIR spectral study of a $\perp$ vibrational band would be the most helpful in learning more about the molecular structure of BeB_2H_8.

In the second part of this work, the high resolution CARS technique was applied for two studies. First, the

newly developed low frequency CARS apparatus at OSU was used to measure the pure rotational Raman spectrum of ethane. The S(J) lines of the ground state and the first torsionally excited state were resolved for the first time. Individual lines from J=10 to J=30 were measured at 300 K and about 200 Torr and analyzed to give rotational constants of B=0.663028(62), 0.660385(48), and D_J=1.066(25)x10^{-6}, 1.031(21)x10^{-6} cm^{-1} for the ground state and the first torsionally excited state, respectively. These values are in excellent agreement with indirect values recently deduced from a high resolution rovibr ational IR study.

Finally, the high resolution CARS apparatus was used to study the ν_3 C-C symmetric stretching mode. Fermi resonance interaction of the ν_3 torsional sublevels with their counterparts of $4\nu_4$ was found to be the reason for the rich and complex spectrum in the ν_3 region. Cold jet spectra and proper accounting of the nuclear spin weights enabled the successful analysis of the spectrum. The results gave ν_3 band origins of 993.612(3), 994.685(4), 994.699(4) and 994.794(3) cm^{-1} for A_{3d}, A_{1s}, E_{3d} and E_{3s} torsional sublevels, respectively. Values of 0.0062106(86) and 0.003274(51) were obtained for α_B and α_A, respectively, which were combined with the ground state rotational constants to yield A=2.670948(51) and B=0.6568173(90)for ν_3.

HIGH RESOLUTION SPECTROSCOPY OF BeB_2H_8 AND C_2H_6

by

Abdullah A. Al-Kahtani

A THESIS

submitted to

Oregon State University

in partial fulfillment of

the requirement for the

degree of

Master of Science

Completed December 2, 1991

Ccommencement June 1992

APPROVED

Redacted for Privacy

Professor of Chemistry in charge of major

Redacted for Privacy

Head of Department of Chemistry

Redacted for Privacy

Dean of Graduate School

Date thesis is presented December 2,1991

Typed by researcher for Abdullah Al-Kahtani

ACKNOWLEDGEMENT

I would like to take the opportunity to thank those people who help me finish this work. I would like to thank Dr. Joseph W. Nibler, my research adviser, for his guidance, support, and outstanding patience. I have always been grateful for being a student of such a bright, creative and enthusiastic teacher.

I also want to thank Mansour Zahedi and Dr. Kirk Brown for their help with the calculation programs and their technical assistance in operating the high resolution CARS apparatus. Finally, many thanks go to every member of our group. I really appreciate their helpful discussions and their contribution to a friendly atmosphere that is fun to be in. My best wishes to each and every one of them.

TABLE OF CONTENTS

LIST OF FIGURES

Figure

LIST OF FIGURES (cont.)

LIST OF TABLES

LIST OF TABLES (cont.)

HIGH RESOLUTION SPECTROSCOPY OF BeB_2H_8 AND C_2H_6

CHAPTER I

VIBRATIONAL ROTATIONAL SPECTRA OF BeB_2H_8

A: Introduction

The determination of the molecular structure of beryllium borohydride (BeB_2H_8) has been one of the most persistent and intriguing problems in structural inorganic chemistry. The molecule was first synthesized by Burg and Schlesinger in 1940[1] via the reactions

$$Be(CH_3)_2 + B_2H_6 \rightarrow CH_3BeBH_4$$

$$CH_3BeBH_4 + B_2H_6 \rightarrow Be(BH_4)_2$$

They reported a vapor pressure of about 6 mm at room

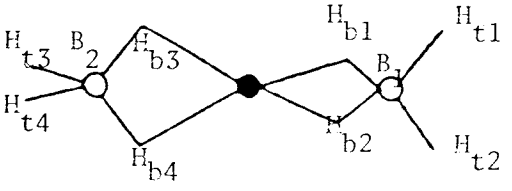

I. D_{2D}

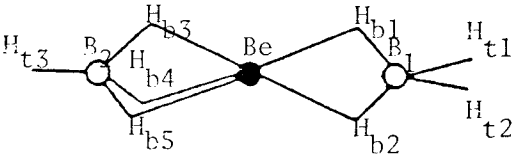

II. C_s

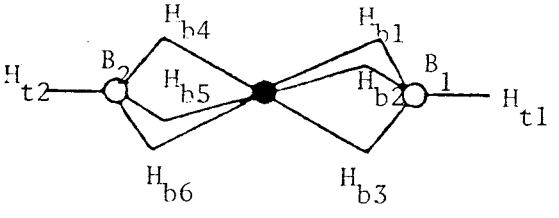

III. D_{3D}

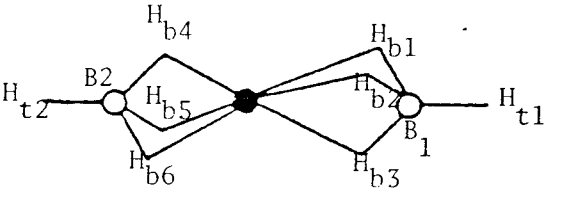

IV. C_{3v}

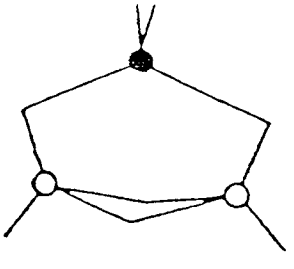

V. C_{2v}

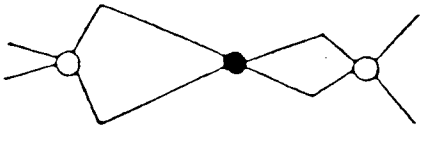

VI. C_{2v}

Figure I,1: Some of the different proposed structures for BeB_2H_8. Atoms are labelled in I, II, III, and IV for a later use.

temperature and a vapor density measurement that suggested a monomeric species in the gas phase. The monomeric nature of the gas phase was confirmed later by Nibler[2]. Burg and Schlesinger reported also that the crystalline phase might be polymeric, and this was confirmed later by a single-crystal X-ray diffraction experiment[3].

To date many unique structures have been proposed, all of which have had some kind of purported experimental verification. The first infrared investigation was carried out by Longuet-Higgins and Bell in 1943[4]. They proposed a structure with douple hydrogen bridges and a D_{2d} symmetry (structure I figure I,1). A subsequent electron diffraction experiment[5] was said to support such a linear B-Be-B arrangement but with two equivalent sets of triple hydrogen bridges having D_{3d} symmetry (structure III figure I,1). However, a few years later the electron diffraction data were reinterpreted and said to be consistent with the infrared double bridged geometry if the bridge hydrogens were allowed to be unsymmetrical[5]. In most standard inorganic texts, the D_{2d} structure became favored and this was not questioned for more than fifteen years.

In 1967 the electron diffraction experiment was repeated and, surprisingly, found to be consistent with a C_{2v} structure[43] (structure V figureI,1). The radial distribution curve was considerably different from the

earlier ones and gave no indication of a long boron-boron distance. This nonpolar structure gained favor when Nibler and Dyke did an electric deflection experiment in 1972 and reported a dipole moment of 2.06±0.12 D[6]. With such a large dipole moment, the symmetrical structures D_{2d} and D_{3d} were apparently eliminated since the dipole moment is forbidden by symmetry for these two structures. Another electron diffraction experiment was done in 1973 by Hedberg et al and yet another different radial distribution curve was obtained[8]. The data did not agree with either the 1946 or the 1967 results. A fit of the data was found to support a D_{3d} structure or a new structure with a C_{3v} symmetry (structure IV figure I,1), which can be derived from the D_{3d} structure by displacing one of the boron atoms toward the beryllium atom.

About the same period, two groups reported two detailed infrared studies of the gas phase. Morgan and Cook[7] reported infrared spectra and assumed that some peaks represented resolved rotational contours. They interpreted the spectra in term of structure having C_{2v} symmetry. About two years later Nibler reported an infrared and Raman study of the gas phase and matrix isolated compound[2]. The spectra were interpreted differently, with all observed peaks treated as vibrational transitions.

An important result reported in Nibler's paper was

evidence that the molecule in the gas phase has at least two structures. Frequencies charateristic of both rriple and double hydrogen bridges were observwd in the gas phace. The structure of the double-hydrogen-bridged isomer was not determined ,but a D_{2d} symmetry was suggested. However, Nibler assigned a C_{3v} symmetry to the trible-hydrogen-bridged isomer which was characterized by a double-minimum asymmmetric B-Be-B stretching potential. This latter conclusion was supported by several observations. First, the matrix-isolated spectra of the 95% Be-HD_2-B trible deuterated compound contained <u>two different</u> Be-H-B bridge stretch absorptions of comparable intensities at about 2200 cm^{-1}. Since the H atom content was only in these deuterated compounds, this indicated the existance of <u>two types</u> of trible bridge protons. Second, the coincidence of some peaks in the gas phase and the matrix-isolated infrared and Raman spectra implied a structure that has no inversion center. A third reasn favoring such a nonpolar structure was the reported dipole moment.

Beside the experimental work summarized above, several theoretical studies were done. In 1973 a theoretical analysis was reported by Marynick and Lipscomp[10]. They investigated many different possible structures of BeB_2H_8 using a minimal basis of Slater type orbitals (STO's) at the self-consistent field level (SCF). Teir calculations

predicted that D_{2d}, D_{3d}, and C_s structures had relative energies of 0.0, 6.5, and 7.3 Kcal/mol, respectively. Optimization starting with a C_{3v} structure led directly to the D_{3d} structure. During the same year, another theoretical study was reported by Ahlrich[11] who used a "Gaussian" pair approximation (IEPA). He found that D_{2d} structure was the lowest in energy at the SCF level. However, when he included electron correlation, the D_{3d} structure was found to have the lowest energy.

The most recent theoretical work, which motivated this thesis study, was reported by Stanton et al in 1988[11]. They investigated four possible structures of BeB_2H_8 (D_{2d}, D_{3d}, C_{3v}, and C_s). These investigators used a very powerful ab initio theoretical techniques based on Many-Body Perturbation Theory (MBPT). Energies calculated at the MBPT (4) level with a basis set of 85 contracted gaussian functions supported the two structure hypothesis of Nibler. However, a C_{3v} double-minimum structure was found to be less stable than the highly symmetric D_{3d} structure. Moreover, the calculated free energies predicted that the D_{2d} structure is the most stable structure, having 1.1 Kcal/mol less than the D_{3d} structure.

Stanton et al reported harmonic frequencies and infrared intensities which were found to be consistent with the spectra observed by Nibler[2]. These calculated

frequencies were used in the assignment of most of the observed features based on D_{2d} and D_{3d} structures. To show the good agreement between the observed and calculated spectra, the assignment of gas phase infrared and Raman spectral features observed by Nibler[2] and those calculated by Stanton et al[11] for BeB_2H_8 are listed in table I,1. The designation of the fundamentals is consistent with tables III and IV of reference 11 for D_{2d} and D_{3d} isomers, respectively, and table IV of reference 2 for C_{3v} isomer. The isomer number from figure I,1 is given in parentheses.

From the experimental and theoretical work summarized above, it is clear that the molecular structure of BeB_2H_8 is one of the longest unresolved problems in structural inorganic chemistry. Although a great deal of experimental and theoretical work has been done, none of the proposed gas-phase structures can be considered to be established. None of the electron diffraction experiments have been analyzed in terms of a two-structure hypothesis. Moreover, the reported dipole moment of 2.06±.12 D has been questioned. While there is no dipole moment for D_{2d} or D_{3d} structures because of symmetry, Stanton et al calculated the dipole moment for C_{3v} structure using two arrangements of the heavy atom nuclei. The first calculation was done using r(Be-B) obtained by the electron diffraction experiment[8]

Table I,1: BeB_2H_8 Gas phase infrared and Raman spectral features observed by Nibler[2] and calculated by Stanton et al using MBPT (2) technique[11].

ν(obs) cm^{-1}	ν(calc)	I(obs)	I(calc) km/mol	Assignment Ref(11)	Assignment Ref(2)
Infrared					
2624	2783	m	82	ν_6(III)	ν_1(IV)
2550	2733	m	142	ν_{14}(I)	....
2500	2639	m	109	ν_9(I)	....
2225	2337	m	303	ν_{14}(III)	ν_{10}(IV)
2167	2335	s	256	ν_7(III)	ν_4(IV)
2071	2122	s	348	ν_{10}(I)	....
2000	2097	w	216	ν_{15}(I)	....
1548	1722	s	1028	ν_{11}(I)	....
1247	1303	w	128	ν_8(III)	ν_{14}(IV)
1130	1152	w	26	ν_{16}(III)	ν_5(IV)
1050	1118	vs	786	ν_9(III)	ν_7(IV)
1000	1004	vs	101	ν_{13}(I)	....
287	287	w	50	ν_{18}(III)	ν_{18}(IV)
Raman					
2627	2782	m (p)	...	ν_1(III)	ν_2(IV)
2550	2733	m	...	ν_{14}(I)	....
2490	2641	s (p)	...	ν_1(I)	....
2175	2350	s (p)	...	ν_2(III)	ν_4(IV)
2075	2143	m (p)	...	ν_2(I)	....
1995	2097	w (p)	...	ν_{15}(I)	....
1150	1181	vw	...	ν_4(I)	ν_6(IV)
535	605	s (p)	...	ν_4(III)	ν_8(IV)
384	441	vw	...	ν_4(III)	....

and gave a dipole moment of 0.46 D, more than four times smaller than the reported dipole moment. The second arrangement (r_1(B-Be)=2Å and r_2(Be-B)=1.5Å, which represents their estimate of the limits of plausible beryllium-boron distances, gave a dipole moment of 2.18 D but at a cost of more than 20 Kcal/mol in energy.

The initial infrared and Raman studies were done at relatively low resolution (0.5 to 1 cm^{-1}) so no vibrational-rotational structure was discerned. Since that time, the resolution improvements to ~0.01 cm^{-1} and even 0.002 cm^{-1} have occurred. Therefore, in this thesis work, we undertook some calculations of the vibrational rotational spectra of the most probable conformers of the molecule to judge whether a repeat of the infrared and Raman experiments at high resolution might be worthwhile in giving new insight into the structure of BeB_2H_8. Accordingly, in section B the rotational constants of the most four probable conformers, D_{2d}, D_{3d}, C_s, and C_{3v}, are calculated. In section C the nuclear spin statistical weights, which play a role in the alternation of the line intensities, are calculated for all conformers except C_s. In section D we discuss the results and our conclusions.

B: Rotational Constants

To predict the vibrational-rotational spectra of a compound, it is necessary to calculate the rotational constants. The mass distribution of any molecule can be described completely by three moments of inertia along mutually perpendicular axes. The selection of such axes is somewhat arbitrary and the mathematical analysis to obtain rotational constants can be simplified by the following systematic approach.

For any rigid molecule, the moment of inertia about an axis passing through the center of mass is given by

$$I = \sum_i m_i r_i^2$$

where r_i is the perpendicular distance from mass m_i to the axis. The so-called momental ellipsoid of the molecule can be formed if a point is plotted a distance along this axis equal to $1/I^{1/2}$ from the center of mass. This procedure then can be repeated for other possible axes through the center of mass. The locus of these points is the surface of an ellipsoid of which the three axes correspond to the principal axes of inertia of the molecule.

The principal axes and the principal moment of inertia can be calculated without a laborious procedure even if the choice of the principal axes is not obvious from the

symmetry of the molecule. For an arbitrary set of cartesian coordinates, The moments of inertia are defined as

$$I_{xx} = \sum_i m_i(y_i^2+z_i^2) \tag{I,2}$$

$$I_{yy} = \sum_i m_i(x_i^2+z_i^2) \tag{I,3}$$

$$I_{zz} = \sum_i m_i(x_i^2+y_i^2) \tag{I,4}$$

and the products of inertia are given by

$$I_{xy} = \sum_i m_i x_i y_i \tag{I,5}$$

$$I_{xz} = \sum_i m_i x_i z_i \tag{I,6}$$

$$I_{yz} = \sum_i m_i y_i z_i \tag{I,7}$$

The moments of inertia that correspond to the center of mass coordinates are given by

$$I^o_{xx} = I_{xx} - M(\overline{Y}^2+\overline{Z}^2) \tag{I,8}$$

$$I^o_{yy} = I_{yy} - M(\overline{X}^2+\overline{Z}^2) \tag{I,9}$$

$$I^o_{zz} = I_{zz} - M(\overline{X}^2+\overline{Y}^2) \tag{I,10}$$

$$I^o_{xy} = I_{xy} - M\,\bar{X}\,\bar{Y} \qquad \text{(I,11)}$$

$$I^o_{xz} = I_{xz} - M\,\bar{X}\,\bar{Z} \qquad \text{(I,12)}$$

$$I^o_{yz} = I_{yz} - M\,\bar{Y}\,\bar{Z} \qquad \text{(I,13)}$$

where

$$M = \sum_i m_i \qquad \text{(I,14)}$$

$$\bar{X} = \frac{1}{M}\sum_i m_i x_i \qquad \text{(I,15)}$$

$$\bar{Y} = \frac{1}{M}\sum_i m_i y_i \qquad \text{(I,16)}$$

$$\bar{Z} = \frac{1}{M}\sum_i m_i z_i \qquad \text{(I,17)}$$

For any molecule, the surface of the momental ellipsoid is generated by[12]

$$I^o_{xx}x^2+I^o_{yy}y^2+I^o_{zz}z^2-2(I^o_{xy}xy+I^o_{xz}xz+I^o_{yz}yz = 1 \qquad \text{(I,18)}$$

The left side of this equation is of real quadratic form which can be rewritten as a matrix equation

$$xI_{xyz}x = 1 \qquad \text{(I,19)}$$

where x is the column vector with elements x, y, z and I_{xyz}, the inertia tensor, is the symmetric matrix

$$I_{xyz} = \begin{vmatrix} I^o_{xx} & I^o_{xy} & I^o_{xz} \\ I^o_{yx} & I^o_{yy} & I^o_{yz} \\ I^o_{zx} & I^o_{zy} & I^o_{zz} \end{vmatrix} \qquad \text{(I,20)}$$

It can be shown that the principal moments of inertia I_a, I_b, and I_c are the roots of this determinantal equation[12]

$$\begin{vmatrix} I^o_{xx}-I & -I^o_{xy} & -I^o_{xz} \\ -I^o_{yx} & I^o_{yy}-I & -I^o_{yz} \\ -I^o_{zx} & -I^o_{zy} & I^o_{zz}-I \end{vmatrix} = 0 \qquad \text{(I,21)}$$

The rotational constants A, B, and C are defined as

$$A = \frac{\hbar}{4\pi I_a}, \quad B = \frac{\hbar}{4\pi I_b}, \quad C = \frac{\hbar}{4\pi I_c} \qquad \text{(I,22)}$$

Using the method summarized above the rotational constants were calculated for the BeB_2H_8 conformers D_{2d}, D_{3d}, C_s, and C_{3v}. The molecular parameters used in the calculation are the theoretical values of Stanton et al[11] for the first three conformers, and those from the electron

diffraction experiment[8] for the C_{3v} conformer. These parameters are collected in table I,2. The calculations was carried out using a computer program which takes the atomic mass and the cartesian distances of each atom from an initial axes choice as inputs and gives the moments of inertia and the corresponding rotational constants as outputs. The calculated cartesian distances for each atom from the principal axes are listed in tables I,3, I,5, I,7, and I,9, while the resultant moments of inertia and rotational constants are collected in tables I,4, I,6, I,8, and I,10 for D_{2d}, D_{3d}, C_s, and C_{3v}, respectively. It can be noticed that there are three different sets of rotational constants for each conformer. The reason is that the abundance of boron is about 80% ^{11}B to 20% ^{10}B. Since the molecule contains two boron atoms, there are three possibilities: $^{11}B_2$ (64%), $^{10}B^{11}B$ (32%), and $^{10}B_2$ (4%).

Table I,2: Structural parameters used in the calculation of the rotational constants.

D_{2d}		D_{3d}	
r(Be-B)	1.857	r(Be-B)	1.734
r(Be-H_b)	1.478	r(Be-H_b)	1.607
r(B-H_b)	1.288	r(B-H_b)	1.254
r(B-H_t)	1.195	r(B-H_t)	1.181
r(H_t-H_t)	2.076		

C_s		C_{3v}	
r(Be-B_1)	1.725	r(Be-B_1)	1.844
r(Be-B_2)	1.875	r(Be-B_2)	1.744
r(Be-H_{b1})	1.659	r(B_2-H_{t2})	1.162
r(Be-H_{b2})	1.565	r(B_1-H_{t1})	1.162
r(Be-H_{b3})	1.511	r(B_2-H_{b2})	1.247
r(B_1-H_{b1})	1.247	r(B_1-H_{t1})	1.363
r(B_1-H_{b2})	1.269	r(Be-H_{b2})	1.549
r(B_2-H_{b3})	1.273	r(Be-H_{b1})	1.772
r(B_1-H_{t1})	1.182	r(Be-H_{t2})	2.906
r(B_2-H_{t2})	1.197	r(Be-H_{t1})	3.006
r(B_2-H_{t3})	1.197	∠(H_{t1}-B_1-H_{b1})	117.65
r(H_{b1}-H_{b1})	1.958		
r(H_{b3}-H_{b3})	2.042		
∠(Be-B_1-H_{t1})	175.8		
∠(Be-B_2-H_{t2})	118.4		
∠(Be-B_2-H_{t3})	121.3		
∠(B_2-Be-B_1)	179.5		

Table I,3: Calculated distances of the atoms from the principal axes for the D_{2d} isomer of BeB_2H_8.

Element	X	Y	Z
Be	0	0	0
B_1	1.875	0	0
B_2	-1.875	0	0
H_{t1}	2.449	1.038	0
H_{t2}	2.449	-1.038	0
H_{t3}	-2.449	0	1.038
H_{t4}	-2.449	0	-1.038
H_{b1}	1.070	0	1.020
H_{b2}	1.070	0	-1.020
H_{b3}	-1.070	1.020	0
H_{b4}	-1.070	-1.020	0

Table I,4: Calculated moments of inertia and rotational constants for the D_{2d} isomer.

Isotope	Moment of Inertia amu Å^2	Rotational constant cm^{-1}
$Be^{11}B_2H_8$	I_a = 8.5343 I_b =110.4718 I_c =110.4718	A = 1.9753 B = 0.1526 C = 0.1526
$Be^{11}B^{10}BH_8$	I_a = 8.5343 I_b =106.8774 I_c =106.8774	A = 1.9753 B = 0.1577 C = 0.1577
$Be^{10}B_2H_8$	I_a = 8.5343 I_b =103.4661 I_c =103.4661	A = 1.9753 B = 0.1629 C = 0.1629

Table I,5: Calculated atom distances from the principal axes for the D_{3d} isomer.

Element	X	Y	Z
Be	0	0	0
B_1	1.734	0	0
B_2	-1.734	0	0
H_{t1}	2.917	0	0
H_{t2}	-2.917	0	0
H_{b1}	1.158	1.114	0
H_{b2}	1.158	-0.557	-0.965
H_{b3}	1.158	-0.557	0.965
H_{b4}	-1.158	0.557	0.965
H_{b5}	-1.158	0.557	-0.965
H_{b6}	-1.158	-1.114	0

Table I,6: Calculated moments of inertia and rotational constants for the D_{3d} isomer.

Isotope	Moment of inertia amu Å^2	Rotational constant cm^{-1}
$Be^{11}B_2H_8$	I_a = 7.5042 I_b = 95.2194 I_c = 95.2194	A = 2.2464 B = 0.1770 C = 0.1770
$Be^{11}B^{10}BH_8$	I_a = 7.5042 I_a = 92.1452 I_c = 92.1452	A = 2.2464 A = 0.1829 C = 0.1829
$Be^{10}B_2H_8$	I_a = 7.5042 I_b = 89.2277 I_c = 89.2277	A = 2.2464 B = 0.1889 C = 0.1889

Table I,7: Calculated atom distances from the principal axes for the C_s isomer.

Element	X	Y	Z
Be	0	0	0
B_1	-1.725	0	0
B_2	1.875	0.016	0
H_{t1}	-2.904	0.087	0
H_{t2}	2.444	-1.053	0
H_{t3}	2.497	1.023	0
H_{b1}	-1.300	-0.575	0.979
H_{b2}	-1.106	1.108	0
H_{b3}	1.114	0.013	1.021
H_{t4}	1.114	0.013	-1.021

Table I,8: Calculated moments of inertia and rotational constants for the C_s isomer.

Isotope	Moment of inertia amu Å^2	Rotational constant cm^{-1}
$Be^{11}B_2H_8$	I_a = 8.1169 I_b =102.8823 I_c =102.8823	A = 2.0769 B = 0.1639 C = 0.1639
$Be^{10}B_2H_8$	I_a = 8.1169 I_b = 96.3749 I_c = 96.4256	A = 2.0769 B = 0.1749 C = 0.1748
$Be^{10}B^{11}BH_8$	I_a = 8.1169 I_b = 99.5691 I_c = 99.6199	A = 2.0169 B = 0.1693 C = 0.1692
$Be^{11}B^{10}BH_8$	I_a = 8.1169 I_b = 99.4685 I_c = 99.5192	A = 2.0169 B = 0.1695 C = 0.1694

Note that this molecule is accidentally a symmetric top.

Table I,9: Calculated atom distances from the principal axes for the C_{3v} isomer.

Element	X	Y	Z
Be	0	0	0
B_1	1.744	0	0
B_2	-1.844	0	0
H_{t1}	2.906	0	0
H_{t2}	-3.006	0	0
H_{b1}	1.114	1.076	0
H_{b2}	1.114	-0.538	0.932
H_{b3}	1.114	-0.538	-0.932
H_{b4}	-1.270	0.618	-1.070
H_{b5}	-1.270	0.618	1.070
H_{b6}	-1.270	-1.236	0

Table I,10: Calculated moments of inertia and rotational constants for the C_{3v} isomer.

Isotope	Moment of inertia amu Å^2	Rotational constant cm^{-1}
$Be^{11}B_2H_8$	I_a = 8.1214 I_b =101.1541 I_c =101.1541	A = 2.0757 B = 0.1667 C = 0.1667
$Be^{10}B_2H_8$	I_a = 8.1214 I_b = 94.1214 I_c = 94.7405	A = 2.0757 B = 0.1779 C = 0.1779
$Be^{10}B^{11}BH_8$	I_a = 8.1214 I_b = 97.8900 I_c = 97.8900	A = 2.0757 B = 0.1722 C = 0.1722
$Be^{11}B^{10}BH_8$	I_a = 8.1214 I_b = 97.8369 I_c = 97.8369	A = 2.0757 B = 0.1723 C = 0.1723

C: Nuclear Spin Statistical Weights

In order to estimate intensities in the vibration-rotation spectra, it is necessary to calculate the nuclear spin statistical weights. The calculation in this section follows the method outlined by Weber[13,14]. Weber shows a procedure in which one can calculate the nuclear spin statistical weight for any symmetric top molecule that belongs to any of the symmetric groups D_{nh}, D_{nd}, C_{nv}, or C_{nh} for $n \geq 2$ for the D point groups and $n \geq 3$ for the C point groups.

The calculation of the weights for the energy levels of any molecule involves three steps. First of all, the symmetry species of the "rovibronic" levels as a function of the different quantum numbers need to be determined. Second, one needs to determine the overall species that are allowed by the Pauli exclusion principle. Finally, one needs to find the character of the nuclear spin representation. The result of Weber's work, therefore, is presented in three sets of tables that give the rovibronic species, the overall allowed species, and the statistical weight. We will utilize these tables as needed; for more detail the reader is referred to the references where the procedure is fully discussed by the author.

As mentioned by Weber, to derive the weights, it should

be noticed that the atoms that form a molecule belonging to a known point group must distribute themselves into a finite number of types depending on their location with respect to the symmetry elements of that group. The atoms that belong to a different type occur in symmetrically equivalent sets which form polygons, pairs of polygons, pairs of atoms, or just a single atom. The definition of the various types of atoms that may compose molecules belonging to the point groups mentioned above are given in references 13 and 14.

The nuclear spin statistical weight of a given rovibronic level is obtained by evaluating the direct product

$$\Gamma_{total} = \Gamma_{EVR} \otimes \Gamma_s \qquad \text{(I,23)}$$

where Γ_s is the representation of all possible nuclear spin functions, and can be expressed in terms of the irreducible representation Γ_s^{α} of the point group S. That is

$$\Gamma_s = \sum_{\alpha} m_{\alpha} \Gamma_S^{\alpha} \qquad \text{(I,24)}$$

Here α is the species label and m_{α} can be evaluated using the standard reduction formula

$$m_{\alpha} = \frac{1}{h} \sum_{c} n_c \chi_s(c) \chi_S^{\alpha}(c) \qquad \text{(I,25)}$$

where h is the order of the group, n_c is the number of elements in the class C, $\chi_s(c)$ is the character of Γ_s, and

χ_s^{α} is the character of Γ_s^{α}. The nuclear spin statistical weight (g_{ns}) is given by

$$g_{ns} = \sum m_{\alpha} \qquad (I,26)$$

In equation (26) it should be noticed that the sum extends only over those terms that contribute to the overall allowed species[13]. General expressions for g_{ns} are given in references 13 and 14. Moreover, references 13 and 14 give the characters of Γ_s for the representative operations of the point groups mentioned above and will be used in the following calculations.

Using the procedure summarized above, the numerical values of g_{ns} have been calculated for the conformers D_{2d}, D_{3d}, and C_{3v}. The final results are collected in table I,11. To show how the calculation was done we give the following example.

Consider the D_{3d} conformer (Figure I,1). In this conformer there is one set of type 1 atoms (Be atom), there are two sets of type 2 atoms (two B atoms and two H_t atoms), and there is one set of type 4b atoms (six H_b atoms). The overall allowed species are[13] A_{2g}^- and A_{2u}^+. From the character table of the point group D_{3d}[15] the nuclear spin characters are[13]

$$\chi_s(E) = (2I_{Be}+1)(2I_B+1)^2(2I_H+1)^8,$$

$$\chi_s(C_3) = (2I_{Be}+1)(2I_B+1)^2(2I_H+1)^4,$$

$$\chi_s(C_2) = (2I_{Be}+1)(2I_B+1)(2I_H+1)^4,$$

$$\chi_s(i) = (2I_{Be}+1)(2I_B+1)(2I_H+1)^4,$$

$$\chi_s(S_6) = (2I_{Be}+1)(2I_B+1)(2I_H+1)^2,$$

and $$\chi_s(\sigma_d) = (2I_{Be}+1)(2I_B+1)^2(2I_H+1)^6. \qquad (I,27)$$

The nuclear spin statistical weight are[13]

for K = 0 and J = even $g_{ns} = m_{A1g}+m_{A1u}$,

for K = 0 and J = odd $g_{ns} = m_{A2g}+m_{A2u}$,

for K = 3p (3,6,9,...) $g_{ns} = (m_{A1g}+m_{A1u})+(m_{A2g}+m_{A2u})$,

and for K = 3p±1 (1,2,4,5,..) $g_{ns} = m_{Eg}+m_{Eu}$. (I,28)

Using the character table and the reduction formula we have

$$m_{A1g}+m_{A1u} = \frac{1}{6}[\chi_s(E)+2\chi_s(C_3)+3\chi_s(C_2)]$$

$$m_{A2g}+m_{A2u} = \frac{1}{6}[\chi_s(E)+2\chi_s(C_3)-3\chi_s(C_2)] \qquad (I,29)$$

$$m_{Eg}+m_{Eu} = \frac{1}{3}[\chi_s(E)-\chi_s(C_3)]$$

For $I_{Be}=3/2$, $I_{B(11)}=3/2$, and $I_H=1/2$ we have the following results

for K = 0 J = even $g_{ns} = 3200$,

for K = 0 J = odd $g_{ns} = 2944$,

for K = 3p $g_{ns} = 6144$,

and for K = 3p±1 $g_{ns} = 5120$.

These weights are reduced to simple relative weights in

Table I,11: Calculated nuclear spin statistical weights for different structures of BeB_2H_8.

Isomer		g_{ns}	reduced weights
D_{2d}			
	J = even	4096	1.000
K = 0			
	J = odd	4480	1.094
K = 4p or 4p±2		8704	2.125
K = 4p±1		7680	1.875
D_{3d} (^{11}B) (^{11}B)			
	J = even	2944	0.958
K = 0			
	J = odd	3200	1.042
K = 3p		6144	2.000
K = 3p±1		5120	1.667
(^{11}B) (^{10}B)			
K = 0		10752	1.000
K = 3p		21504	2.000
K = 3p±1		17920	1.667
C_{3v} (^{11}B) (^{11}B)			
K = 0		6144	1.000
K = 3p		12288	2.000
K = 3p±1		10240	1.667
(^{11}B) (^{10}B)			
K = 0		10752	1.000
K = 3p		21504	2.000
K = 3p±1		17920	1.667

table I,11. For the most prevalent BeB_2H_8 molecule, it is seen that the C_{3v} and D_{3d} cases differ only in that the K=0 transitions of the latter alternate by 8.7%. A similar alternation (9.4%) is predicted for the K = 0 lines of the D_{2d} structure. Thus very accurate intensity measurements of this K = 0 structure would allow a structural distinction to be made but this will be difficult experimentally.

Perhaps more distinctive is the alternation predicted for different K lines. For the D_{2d} structure, alternating intensities of 1 : 1.13 are predicted for odd : even K values whereas the threefold symmetry of the D_{3d} and C_{3v} structures predicts a repeating alternation of 1 : 1 : 1.20 as K varies from 1 : 2 : 3 and so on. Such an alternation may be helpful, as will be discussed later.

D: Predicted Spectra And Discussion

Energy levels

The main reason for the calculations in the preceding two sections was to obtain parameters to predict the resolved vibration rotation band spectra of different isomers of BeB_2H_8. From such spectra one might hope to draw a conclusion regarding the symmetry of the molecule. We note that the four isomers considered are all essentially symmetric tops. The total energy of vibration and rotation of a symmetric top molecule in a non-degenerate vibrational state is given, approximately, by

$$T = G+F_v(J,K) \qquad (I,30)$$

where G is the vibrational term and $F_v(J,K)$ the rotational term, given by

$$F_v(J,K) = B_vJ(J+1)+(A_v-B_v)K^2-D_JJ^2(J+1)^2-D_{JK}J(J+1)K^2-D_KK^4 \qquad (I,31)$$

B_v and A_v are the average values of the rotational constants for a vibrational level and the D's are (small) centrifugal distortion constants. The infrared and Raman spectra then consist of the transitions among these levels that are allowed by the appropriate selection rules.

Population factors

The major factor in determining the relative intensity

of the rotational fine-structure lines is the relative populations of the rotational levels. The population can be described using the Boltzmann distribution law. The fraction of the population of the level with rotational quantum numbers J and K is

$$\frac{N_{JK}}{N_{total}} = \frac{g_{ns}(2J+1)\, e^{-\frac{E_{JK}}{kT}}}{Q} \qquad (I,32)$$

where the centrifugal distortion terms can be neglected in evaluating E_{JK}. Q, the partition function, is given by

$$Q = \sum_{J=0}^{\infty} \sum_{K=-J}^{K=J} g_{ns}(2J+1)\, e^{-\frac{E_{JK}}{kT}} \qquad (I,33)$$

It can further be shown[17] that Q is given to a good approximation by

$$Q = \frac{\pi^{\frac{1}{2}}}{\sigma}\left(\frac{k^3T^3}{\hbar^3B^2A}\right)^{\frac{1}{2}} \qquad (I,34)$$

where σ is the symmetry number of the molecule (2 for D_{2d}, 3 for D_{3d} and C_{3v}, and 1 for C_s).

Lineshapes

The prediction of the line shape is also important in calculating the convolved spectra of the different isomers. For a molecule in the gas phase, the dominant contribution to the width of a spectral line come from the Doppler effect and intermolecular collisions. The Doppler effect occurs

when a molecule is moving so that the component of its velocity is parallel to the direction of propagation of the radiation field with which it interacts. Averaging over the velocity distribution then gives a half-width at half maximum of[16]

$$\Delta\nu_{dop} = \frac{\nu}{c}\left(\frac{2kT\ln 2}{m}\right)^{\frac{1}{2}} \qquad (I,35)$$

or

$$\Delta\nu_{Dop} = 3.6\times10^{-7}\left(\frac{T}{M}\right)^{\frac{1}{2}}\nu\,(Hz) \qquad (I,36)$$

where M is the molecular weight and ν is the vibrational transition. At room temperature and for a vibrational transition of 2000 cm^{-1}, ν_{Dop} is equal to about .002 cm^{-1} for BeB_2H_8.

The half-width at half maximum caused by uncertainty broadening due to intermolecular collisions is given by[16]

$$\Delta\nu_{col} = \frac{1}{4\pi\tau} \qquad (I,37)$$

where τ is the mean time between collisions which, from gas kinetic theory, is

$$\tau = \frac{1}{\pi\rho^2\bar{\upsilon}N} \qquad (I,38)$$

Here ρ is the collision diameter, N is the concentration, and υ is the average velocity given by

$$\bar{v} = \left(\frac{8kT}{\pi m}\right)^{\frac{1}{2}} \qquad (I,39)$$

The choice of ρ is uncertain but we estimate from geometrical parameters that it would be about 10 Å. For a vapor pressure of 3.4 Torr[6] at room temperature $\Delta\nu_{col}$ would then be about 0.0008 cm^{-1}.

Combining the two effects, each transition line is expected to have a full-width at half maximum of about 0.005 cm^{-1} at room temperature. Further broadening will come from any instrumental limitation in resolution.

Pure Rotational Spectra

We now discuss possible kinds of spectral study that might be performed to distinguish between the different structural isomers of BeB_2H_8. We consider first a pure rotational spectrum which might be obtained by microwave spectroscopy or by Raman study using the high resolution CARS apparatus available at OSU.

We note that a microwave spectrum is not possible for any nonpolar structure such as the D_{2d} or D_{3d} configurations and, further, that some (unpublished) attempts to obtain a microwave spectrum were not successful. This may have been due to the instability of the compound, particularly with metal surfaces present, as is usually the case in microwave spectroscopy. More promising would be the use of high resolution Coherent Raman Spectroscopy, where the sensitivity has now improved to the point that gases at a

few Torr pressure can be studied.

The frequencies of the pure rotational Raman transitions in a totally symmetric state such as the ground vibrational state are obtained by imposing the selection rules $\Delta J = \pm 1, \pm 2$, $\Delta K = 0$, and $J'+J'' \geq 2$. The spectrum then consists of only an R branch and an S branch whose frequencies are given by

$$S(J,K) = (4B-6D_J-4D_{JK}K^2)(J+\frac{3}{2}) - 8D_J(J+\frac{3}{2})^3 \qquad (I,40)$$

$$R(J,K) = 2(B-D_{JK}k^2)(J+1) - 4D_J(J+1)^3 \qquad (I,41)$$

However, since I_a/I_b is small for all conformers considered here (see section B), it is known that the intensity of the R branch would be much less than that of the S branch[17]. Therefore, we will consider here only the latter. If we neglect the centrifugal distortion constants for the moment, the S branch will consist of a series of lines separated by 4B. Calculated stick spectra of this type for the D_{2d} and D_{3d} are shown in figure I,2. Looking at the spectra of figure I,2 and back to the results of section B we see that this predicts a spacing of 0.6104, 0.7080, 0.6556, and 0.6668 cm^{-1} for $Be^{11}B_2H_8$ conformers of D_{2d}, D_{3d}, C_s, and C_{3v}, respectively. This would perhaps suggest that the structures might be distinguished on the basis of these line spacings but, of course, these spacings are determined by the initial choice of structural parameters. We have

examined the effect of small bond length and angle changes on the rotational constants and feel that the problem is indeterminant. For example, a simple, and possible, 8% decrease in the Be-B bond length of the D_{2d} structure would yield the same B value as for the D_{3d} geometry. This illustrates the fact that it will be difficult to distinguish between the different isomers by just considering the difference in their rotational constants.

We next consider the possibility of distinguishing between the different isomers from the intensity alternation among the different K values within a J transition line. This intensity alternation is governed, to some extent, by the nuclear spin statistical weight (g_{ns}) calculated in section C. As mentioned in section C, the g_{ns} values reported in table I,11 suggest that it may be possible to distinguish between a three-fold symmetry axis (D_{3d}, or C_{3v}) and a two-fold symmetry axis (D_{2d}), if different K lines can be resolved. The spacing between different K values within each J transition is given by the $D_{JK}K^2$ term in equation I,40. D_{JK} is unknown, however, a simulation of the expected spectrum was done assuming centrifugal distortion constants of a molecule similar to BeB_2H_8 (Allene with $D_J = 1.1\text{x}10^{-6}$, and $D_{JK} = 4.6\text{x}10^{-6}$ cm^{-1}). In figure I,3 we show the simulation of S(24), the strongest line in the stick spectra of figure I,2, for both the D_{2d} and D_{3d} conformers. In the simulation process, the positions of the different K lines

within the S(24) transition were first calculated and presented by sticks, where we can see the intensity alternation for different K's for both isomers. It is clear from the stick spectra that it is possible to distinguish between the two isomers. A convolution over all K lines was done using the broadening effects discussed earlier. The result, presented by the broad bands in figure I,3, shows that the different K lines are not likely be resolved unless our estimate of D_{JK} is much too low. We conclude then that a pure rotational Raman study of the molecule is unlikely to be of much help in establishing the molecular structure.

Vibrational-Rotational Spectra

Consider now a vibrational infrared study where we have an infrared parallel (∥) band. For such a band, only levels of the same K value combine with one another, i.e. only $\Delta K=0$ transitions occur. For each particular value of K there is a sub-band with three branches P, Q, and R. If the interaction between vibration and rotation and the centrifugal terms are neglected, that is, if B'=B", A'=A", and D_J,...etc = 0, all the sub-bands for different K values coincide. In this case we obtain a band with a strong narrow Q branch, a P branch, and an R branch. The spacing of the lines in the P and R branches is 2B. If we assume centrifugal distortion terms as we did in the pure rotational case and also assume that they are equal for the

ground state and the excited state, we would have a similar spectrum to that of the pure rotational case for the R branch with the exception that the different K values within a J transition are more closely spaced (for an R line the spacing is $2D_{JK}K^2$ instead of $4D_{JK}K^2$). Therefore, similar simulations of the K structure in the R branch spectrum would show that a study of this kind might not help either.

Consider next an infrared perpendicular ($\perp$) band for which the selection rule is $\Delta K = \pm 1$. Here the band also consists of a number of K sub-bands but, even if the interaction of rotation and vibration is neglected, the sub-bands do not coincide. Ignoring (small) coriolis effects, the band origin of each sub-band is given by

$$\nu = \nu_o + (A'-B') \pm 2(A'-B')K + [(A'-B'-(A''-B'')]K^2 \qquad (I,42)$$

where the + sign applies to the $\Delta K=+1$ branch and the - sign applies to the $\Delta K=-1$ branch. If the vibrational rotational interaction is neglected, the lines of the Q branches in each sub-band coincide at ν, and the different Q branches form a series of lines with a spacing of 2(A-B). P and R branches accompany each of these Q "lines" to form a usually unresolved background with a very low intensity compared to the Q branches. This is especially true when $A >> B$[17], as is the case for all conformers considered here. Figure I,4 shows the stick spectra of the D_{2d} and D_{3d} isomers for the lines ${}^RQ_0$ to ${}^RQ_9$ where it can be seen that it may be possible

to distinguish between them from the alternation in the intensity of different K values. Similar results might be obtained by performing a Raman study of non-totally symmetric nondegenerate Raman band. Here, the selection rule is $\Delta K=\pm 2$ and the spectrum is similar to that of a $\perp$ infrared band except that the spacing is now equal to 4(A-B).

In the Raman spectrum of a transition between two totally symmetric vibrational states only $\Delta K=0$ occurs. There will be one series of sub-bands of the same type as for an infrared $\parallel$ band except that there will be the additional O and S branches with a spacing of 4B. Most importantly, the Q branches are much more intense than the O, P, R, or S branches, and, in fact, the Q branch is usually the only part of the band that can be easily observed in Raman spectroscopy[17]. Here, it is possible to study the Q branch using a high resolution apparatus such as the CARS apparatus discussed in chapter II.

For the Q branch ($\Delta J = 0$ and $\Delta K = 0$) the Raman shifts are given by

$$Q_K(J) = \nu_o+(B'-B'')J(J+1)+[(A'-B')-(A''-B'')]K^2 -(D_J'-D_J'')J^2(J+1)^2-(D_{JK}'-D_{JK}'')J(J+1)K^2-(D_K'-D_K'')K^4$$

(I,43) Assuming rotational constant <u>differences</u> of the same order of that of ethane discussed in chapter II, the expected spectra are simulated for the D_{2d} and D_{3d} and shown

in figure I,5. Looking at the K = 2 and K = 3 series we can see that relative intensity of the first is bigger for the D_{2d} conformer while the relative intensity of the second is bigger for the D_{3d} conformer. Therefore, it might be possible to get some information regarding the molecular symmetry from such spectra although this will depend sensitively on the unknown rotational constant differences.

It should be noticed that the actual spectra will differ somewhat from the above simulations due to a variety of factors. For perpendicular bands perturbations will occur due to vibration-rotation interactions and coriolis effects but these will probably be small. Contributions from hot bands of low frequency bending modes may be a more severe problem however since three vibrations fall below 500 cm^{-1} (see table I,1). Implicit in our calculations is that the idea isotopically pure ^{11}B would be used in the synthesis but, to the extent that ^{10}B is present, the spectra will be more complex.

Our conclusion then is that the most useful study of BeB_2H_8 would be to examine Q branch intensities of a $\perp$ band by high resolution FTIR specroscopy. A similar study by CARS is also possible but likely to be more difficult due to the low Raman intensities of $\perp$ nonsymmetric transitions. It is our hope that these calculations will serve as a stimulus to further spectroscopic work on BeB_2H_8 structure.

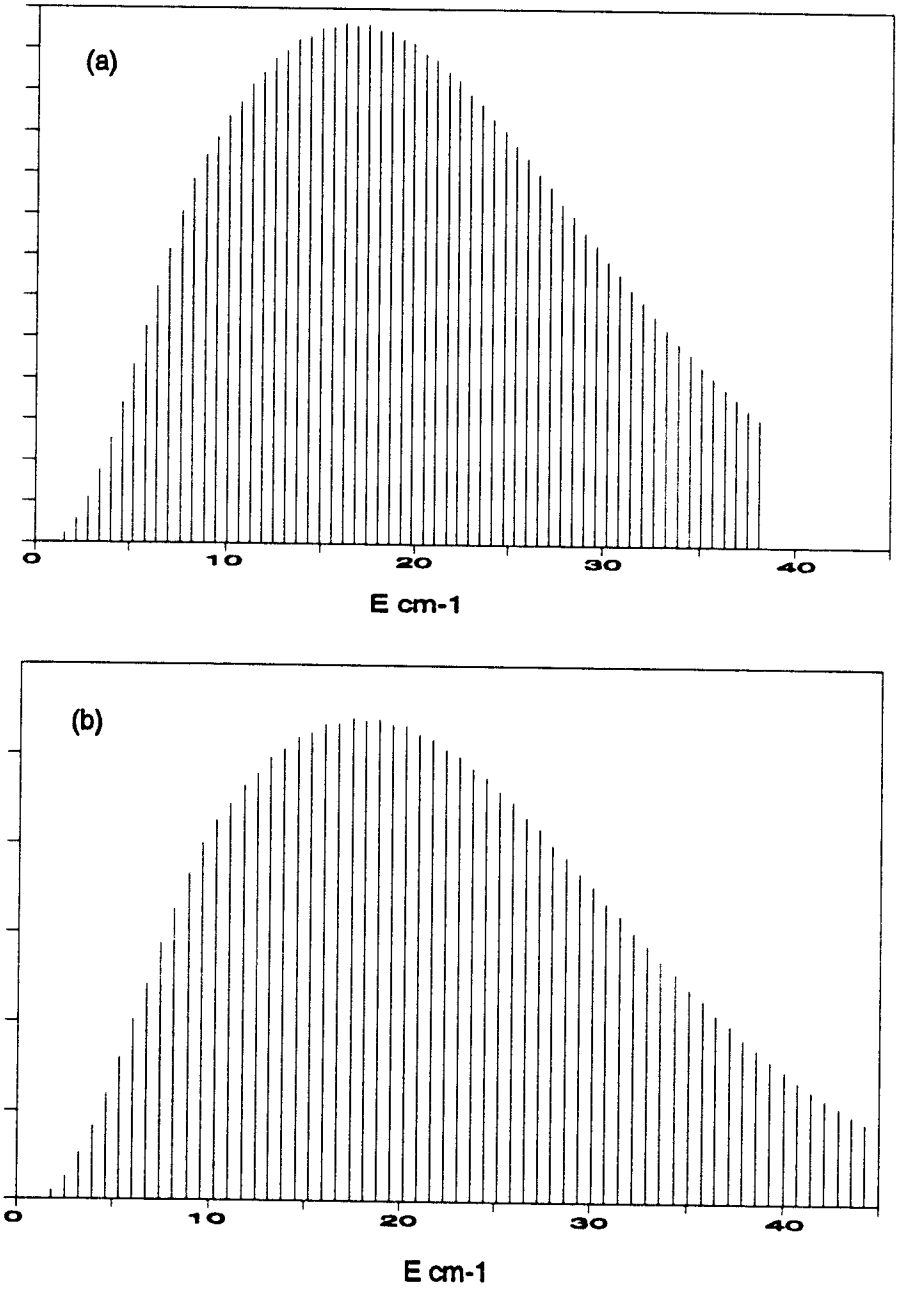

Figure I,2: Predicted pure rotational spectra for the D_{2d} isomer (a) and the D_{3d} isomer (b) at 300 K.

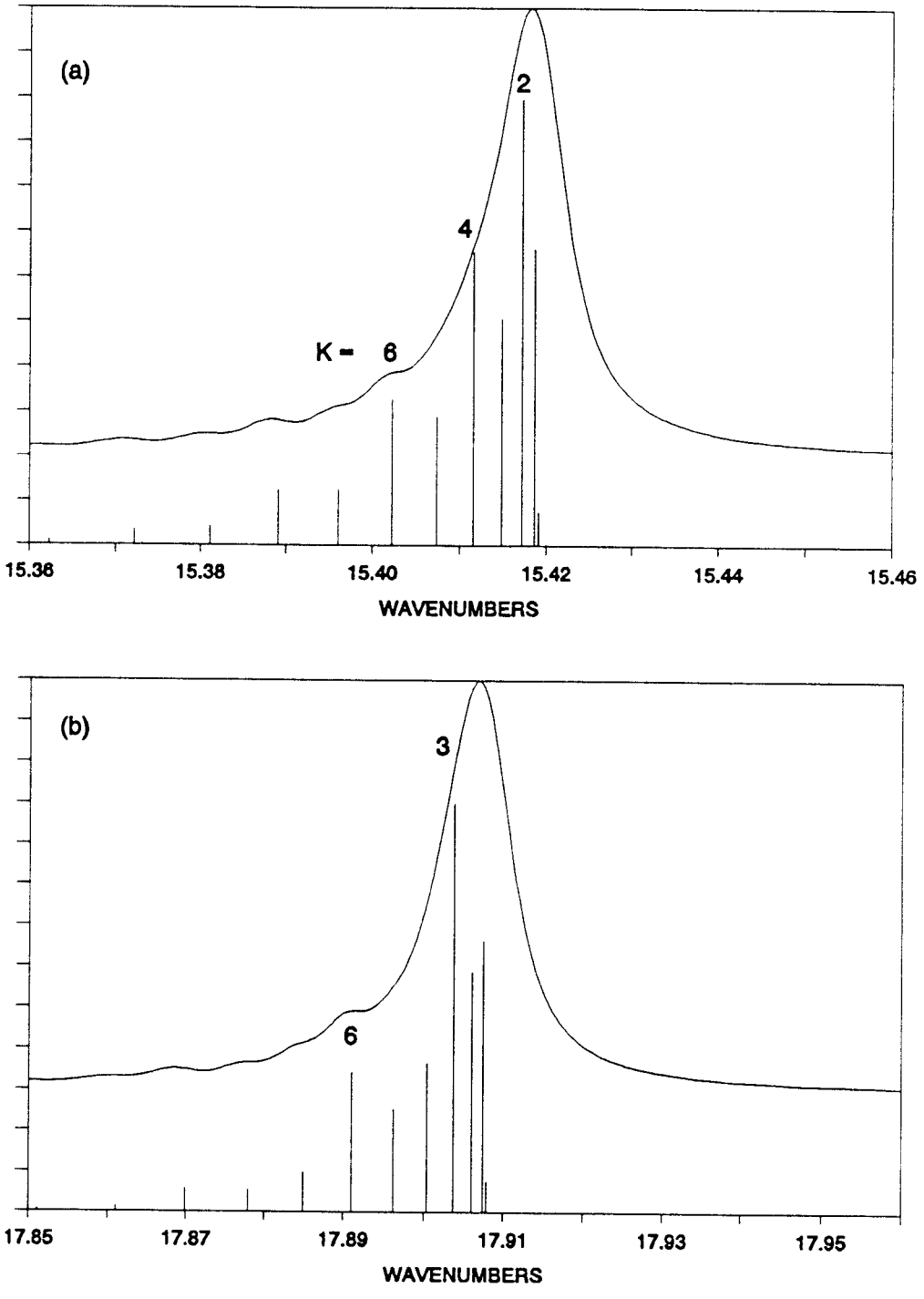

Figure I,3: Simulated spectra for S(24) line of the D_{2d} isomer (a) and of the D_{3d} isomer (b) at 300 K.

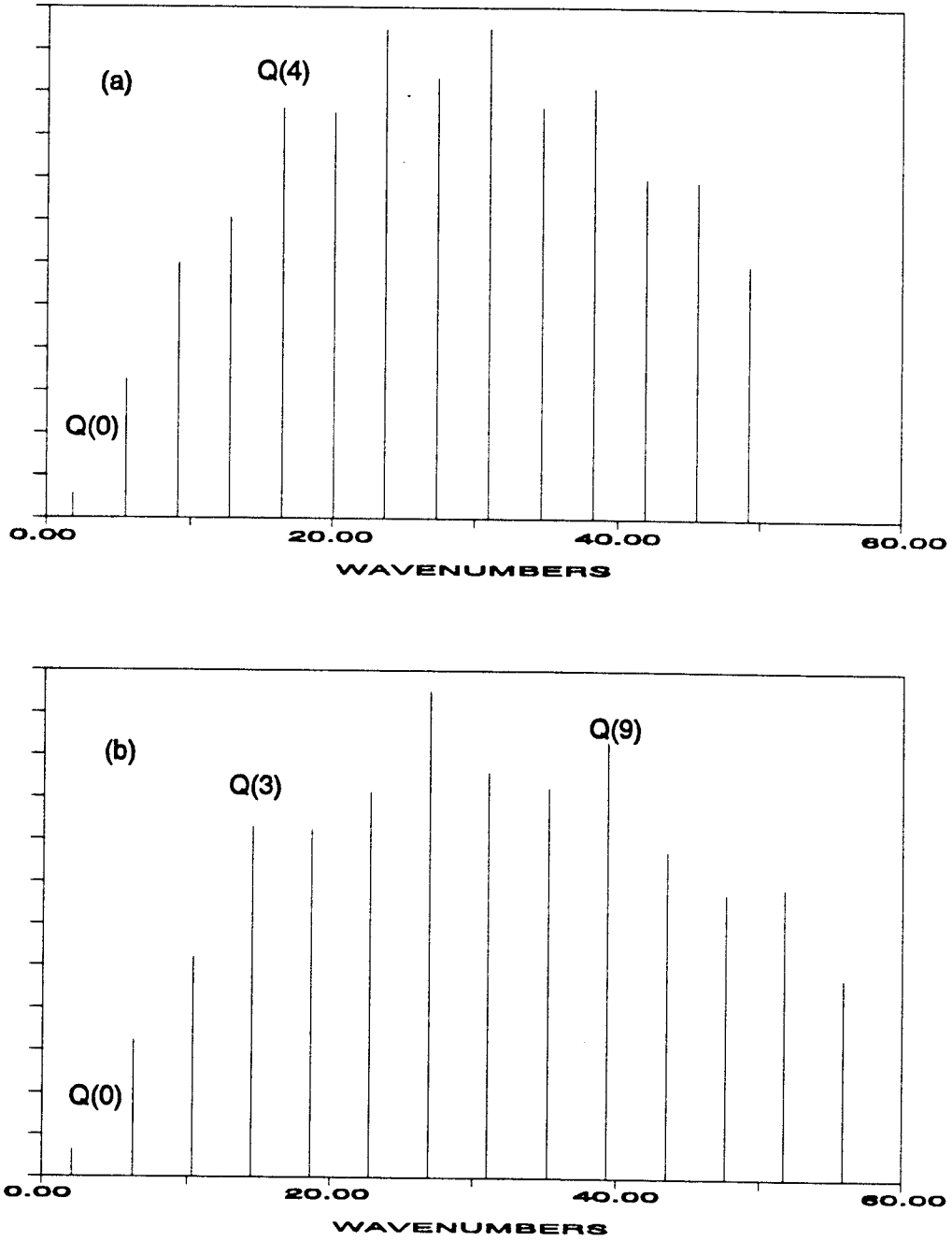

Figure I,4: Spectra of a $\perp$ IR band for the D_{2d} isomer (a) and the D_{3d} isomer (b).

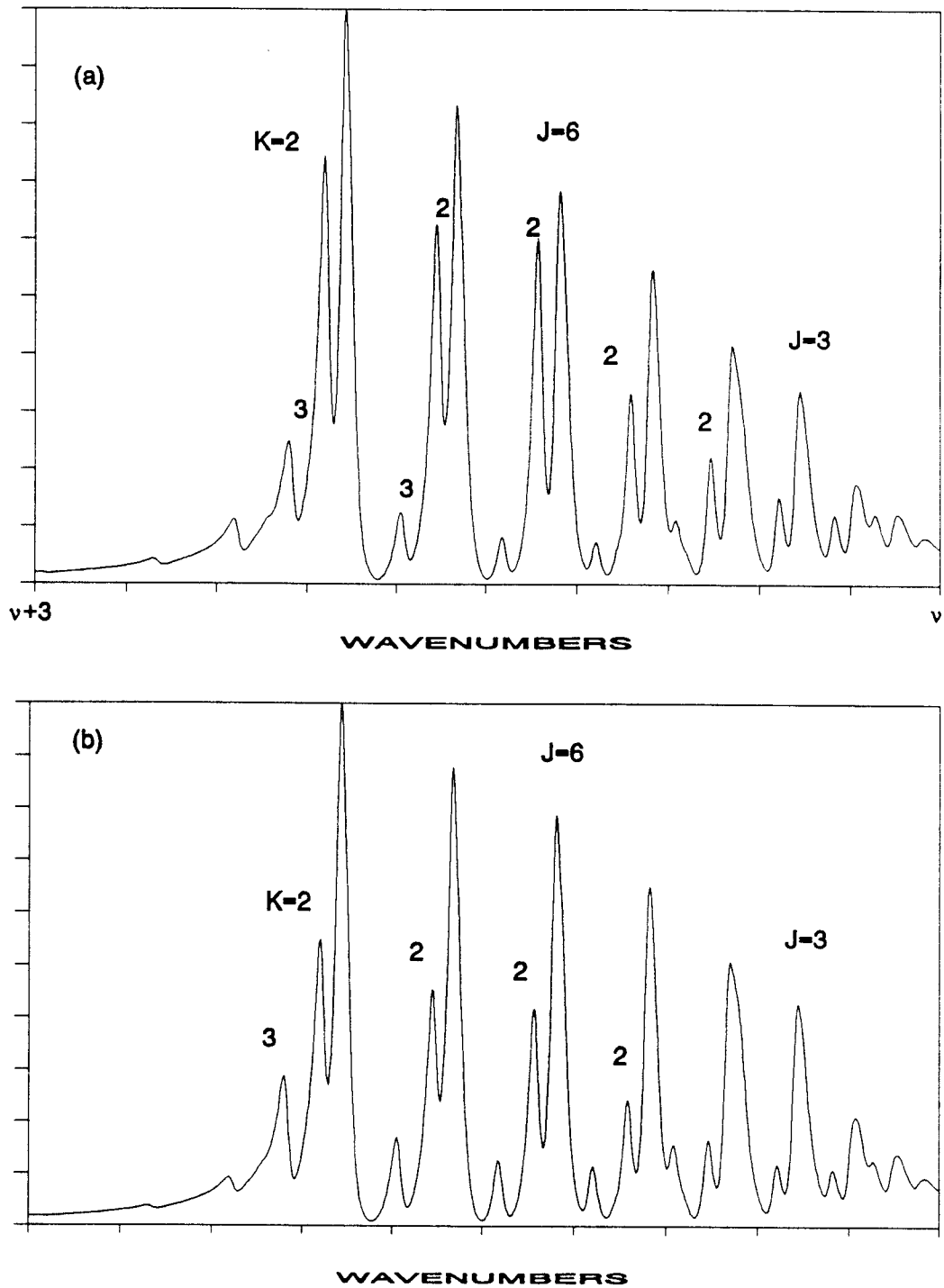

Figure I,5: Simulated spectra of a Q branch for the D_{2d} (a) and D_{3d} (b). at 100 K.

CHAPTER II

HIGH RESOLUTION CARS SPECTRA OF C_2H_6

A. Introduction

This chapter deals with the use of high resolution CARS to obtain both pure rotational and vibrational rotational spectra of ethane. Understanding the spectra of ethane has been of great interest to many spectroscopists for about half a century. This interest stems mainly from the fact that ethane is the prototype for molecules with internal torsional motion and the three-fold potential barrier height and shape have been examined in detail. Understanding the spectra of ethane and reaching a way of interpreting them is expected to aid in the understanding of spectra and torsional potential of other more complicated molecules.

In the last decade, there has also been motivation for studying the spectra of C_2H_6 for astrophysical reasons. Ethane lines have been observed in the atmospheres of Jupiter, Saturn, Titan, and Neptune[38] and properly analyzing the observed spectra can give useful estimates of the local temperatures of the surfaces of these planets. Finally, we note that C_2H_6 is an atmospheric pollutant

resulting from incomplete fossil fuel combustion, and in fact, ethane lines have been used in spectral analysis of the air above Los Angeles[19].

A great deal of theoretical and experimental work has been done with regard to understanding the spectra of ethane. Without attempting to go over this in detail, we summarize some of the results in the following.

We note that some of the infrared and Raman spectra involving the fundamentals and a few combination bands[20-30] were initially analyzed and assigned using the assumption that the molecule is staggered in its equilibrium configuration so as to belong to the D_{3d} point group. However, it was realized early that this approach was not completely valid since the molecule has three equivalent equilibrium configurations which may be interchanged by torsion of one methyl group around the C-C axis[29]. The free rotation around this axis was shown to be impeded by a high torsional barrier[29] leading to the prediction of splitting in the torsional levels. The magnitude of the barrier and the effect of the splittings on the spectra were first examined in an infrared measurement of the torsional mode (ν_4)[29]. In several studies later it was noticed that the presence of such a barrier not only affects ν_4 but, to a lesser extent, all other vibrational modes.

In a very detailed theoretical treatment of the

torsional problem of ethane[30], corrections were made for the fact that the D_{3d} group is not the correct one for ethane. It is true that there are three equivalent reference configurations, all of which belong to the D_{3d} point group, but which are separated by the torsional barrier. However, tunneling through the barrier can mix the levels of these three configurations and a group that contains all three configurations should be used to describe the vibration-rotation-torsion in the molecule overcoming the barrier. Such a group is G_{36} proposed by Longuet-Higgins in 1963[31]. Moreover, since C_2H_6 has two identical CH_3 rotors, another set of three configurations are generated by 180° rotation around the C-C axis. This operation doubles the G_{36} group and generate the G_{36}^+ group which has 72 symmetry elements[30]. This number may be contrasted with the 12 symmetry elements of the D_{3d} group.

Using this theory, the barrier for the internal motion associated with the torsion was recently redetermined from a direct observation of the inactive torsional mode in a high resolution FTIR experiment[32]. The data were fitted to the parameters of the torsional part of the energy Hamiltonian to give 1011.89 cm^{-1} and 10.768 cm^{-1} for V_3 and V_6, the three- and six-fold contributions to the barrier height, respectively. It was estimated later that this high barrier induces splittings which are only very small for the ground (~2 x 10^{-3} cm^{-1}) and the first excited states

(~0.08 cm^{-1})[33]. Observation of these splitting for the ground state thus requires a very high resolution spectrometers. Such resolution is routinely achieved in microwave rotational spectroscopy but, of course, this is not applicable to C_2H_6 since it has no dipole moment. Thus rotational Raman is the only way to directly measure the rotation spectrum.

When these splittings are resolved, the full permutation-inversion group (G_{36}^{+}) of the non-rigid molecules should be used when analyzing the spectra. However, when the splittings are not resolved, as proved the case in our rotational study, the influence of the hindered rotation may be neglected, and the molecule can be assumed, to a good approximation, to remain staggered in its reference configuration[33]. This assumption was made in analyzing the results of rotational study. The second part of this work involved measurements of the ν_3 (C-C stretch) vibration-rotation Q branch structure of C_2H_6 where, as will be seen, the torsion sublevels are observed due to an unusual Fermi resonance tnteraction.

The vibrations of the staggered ethane molecule can be classed according to the D_{3d} point group which contains six irreducible representations, A_{1g}, A_{1u}, A_{2g}, A_{2u}, E_g, and E_u. All but one of the 12 vibrational modes are either infrared or Raman active. The gerade-symmetry vibrational transitions are Raman active while the ungerade-symmetry

vibrational transitions are infrared active. Vibrational transitions which have A_{1u} or A_{2g} symmetry are expected to be inactive. In the Raman spectrum non-degenerate transitions of A species are expected to show vibrational rotational bands obeying the selection rules $\Delta K = 0$ and $\Delta J = 0, \pm 1, \pm 2$, which is the case for ν_3 studied here. Values for the twelve fundamental vibrational frequencies of ethane are collected in table II,1. Here the first column gives the mode labelling, the second gives the symmetry type under the D_{3d} point group, the third gives the approximate mode description, the fourth gives the infrared and Raman selection rules[27,33], and the fifth column gives the band origin collected from the literature and from our work.

In this thesis work, the Coherent Anti-Stokes Raman Scattering (CARS) technique was applied to obtain the first high resolution pure rotational and ν_3 Q-branch Raman spectra of C_2H_6. The remainder of this chapter, then, consists of four sections. In section B, a brief discussion of the CARS technique is given and the experimental arrangement is discussed. In section C, the pure rotational CARS spectra of ethane are presented and analyzed. The somewhat novel and involved analysis of the CARS spectra of the Q branch of ν_3 is given in section D. Finally, discussion of the results and summary are presented in section E.

Table II,1: Properties of the twelve fundamental vibrational modes of C_2H_6.

Mode number	Symmetry in D_{3d}	Mode description	Selection rules	Band origin cm^{-1}
ν_1	A_{1g}	C-H stretch	R $\Delta K=0$	2954.00
ν_2	A_{1g}	CH_3 bend	R $\Delta K=0$	1404.10
ν_3	A_{1g}	C-C stretch	R $\Delta K=0$	994.72
ν_4	A_{1u}	torsion	Inactive	288.85
ν_5	A_{2u}	C-H stretch	IR $\Delta K=0$	2895.70
ν_6	A_{2u}	CH_3 bend	IR $\Delta K=0$	1379.16
ν_7	E_u	C-H stretch	IR $\Delta K=\pm1$	2985.39
ν_8	E_u	CH_3 bendd	IR $\Delta K=\pm1$	1471.39
ν_9	E_u	rock	IR $\Delta K=\pm1$	821.74
ν_{10}	E_g	C-H stretch	R $\Delta K=\pm1, \pm2$	2968.69
ν_{11}	E_g	CH_3 bend	R $\Delta K=\pm1, \pm2$	1468.10
ν_{12}	E_g	rock	R $\Delta K=\pm1, \pm2$	1195.30

B. The CARS Process and the Experimental Arrangement

When applying an electric field to a molecular system, a polarization is induced which is given by

$$P = \chi^{(1)}.E + \chi^{(2)}.E.E + \chi^{(3)}E.E.E + \ldots \qquad (II,1)$$

where E is the electric field and $\chi^{(i)}$ is the dielectric susceptibility tensor. $\chi^{(20)}$ is the lowest order term which is responsible for the different types of nonlinear Raman spectroscopy.

CARS is a four-wave mixing process which has received more attention than other nonlinear Raman techniques. As shown in figure II,1, in the CARS process, a Raman active vibrational or rotational mode of frequency ω_v is excited in the field of two laser beams, ω_1 and ω_2, which are tuned such that $\omega_1 - \omega_2$ matches the molecular resonance. This coherently driven ensemble of oscillators couples with a second ω_1 photon to produce a laser like output at anti-Stokes frequency, $\omega_3 = \omega_1 + \omega_v = 2\omega_1 - \omega_2$.

To produce a strong CARS signal, the incident beams must be aligned and properly phased according to the phase matching condition

$$2k_1 - k_2 - k_3 = 0 \quad (\Delta k = 0) \qquad (II,2)$$

where k_i is the wave vector. There are two common

arrangements for phase matching. One is a collinear arrangement in which all the input beams propagate collinearly in the same direction, resulting in a high signal level due to the long interaction distance. However, with this geometry difficulty in separating the signal from the pump beam is experienced, especially at low Raman shifts where the signal wavelength is very close to the pump beam wavelength.

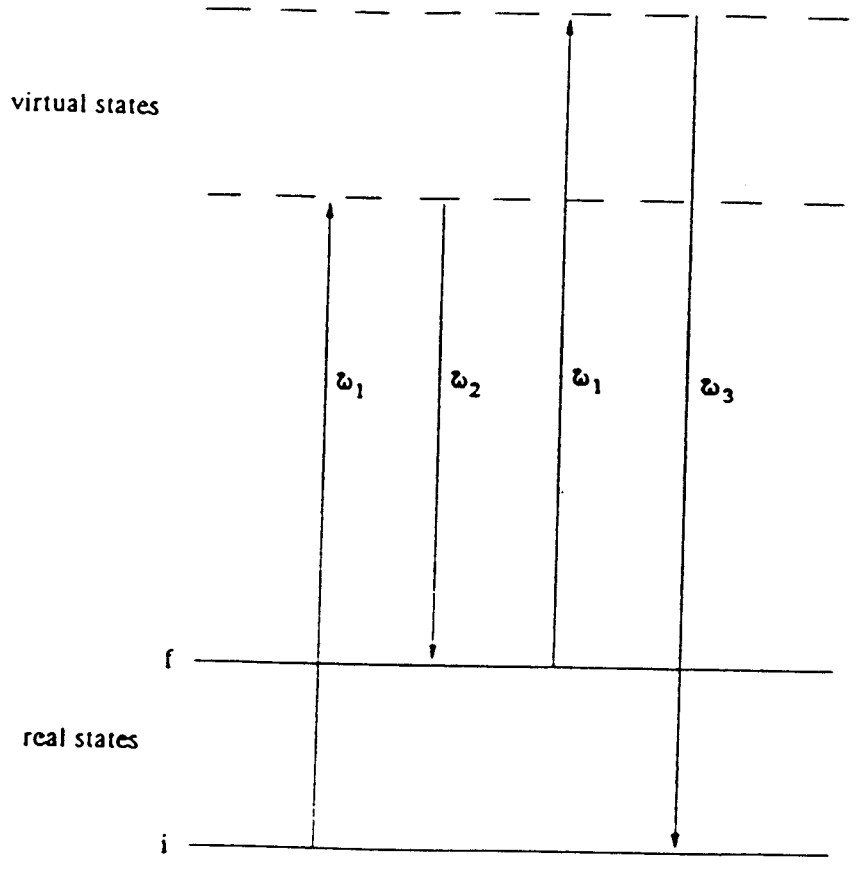

Figure II,1: Resonant interaction in CARS process

The second arrangement, which was employed in this thesis work, is known as the BOXCARS arrangement. Here all beams meet at one point, the focal point of the focusing lens as shown in figure II,2. This method is better than the previous one in the sense that spatially isolation of the signal from other beams is possible which leads to a higher instrumental rejection of ω_1 and ω_2 background. In addition, the nonresonant contributions from the cell walls and the air outside the cell is minimized since the CARS process takes place only at the point of the beams crossing in the middle of the sample cell.

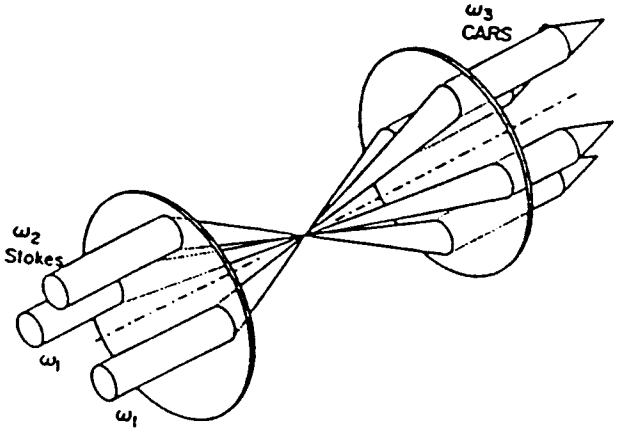

Figure II,2: 3-D plot of folded BOXCARS geometry.

The high resolution CARS apparatus used in this study is shown in figure II,3. The apparatus was modified recently in order to be used in both vibration and pure rotation regions with only a minimal modification in the optical arrangement. The laser used in this apparatus is a Quanta-Ray DCR-1 Nd-YAG laser,which has been retro-fitted with a Lightwave Electronics Model 6300 Injection seeder to give 1.06 μm radiation in 8 ns pulses at 10 Hz. In the case of study in the vibration region, the second harmonic at 532 nm of this laser is split into three portions. Two thirds is used to pump a three-stage dye amplifier chain through which the tunable output of a Coherent 699-29 cw ring dye laser passes. The amplified R6G dye solution beam is then directed , along with the remainder 1/3 portion of the 532 nm beam which has been split into two beams, into the sample cell in a folded BOXCARS arrangement. The resultant CARS signal is spatially filtered, collimated, and directed through a monochromator to a Hamamatsu R955 photomultiplier tube whose output is directed to an SRS Model SR250 gated integrator. Finally, the signal is averaged over 2^n shots using an Apple computer system in which the final data are stored for further analysis.

The Nd-YAG frequency was determined by the cw seed laser whose output was temperature tuned so that the frequency matches the absorption of an I_2 line in a cell. In order to calibrate the Stokes ω_2 frequencies in a scan,

a portion of the ring dye laser output was sent through a 10 cm I_2 cell and the transmission was measured using a photodiode and reported simultaneously with the data. The I_2 frequencies were then calibrated by comparing them with the I_2 atlas values, $\tilde{\omega}_2$ was corrected accordingly, and the desired frequencies were obtained from $\tilde{\omega}_1 - \tilde{\omega}_2$.

For the pure rotational Raman study, the apparatus was modified slightly. As shown in figure II,3, one of the 532 nm input beams is replaced by light at 568.2 nm from a single-mode Coherent Kr^+ ion laser whose output was directed through a three-stage amplifier chain pumped by the green (532 nm). The ring dye amplifier chain was tuned to operate in the range overlapping the Kr^+ line so as to derive rotational transitions coherently. Then the 532 nm source was used as the probe to generate the anti-Stokes signal photons at a slightly shorter wavelength.

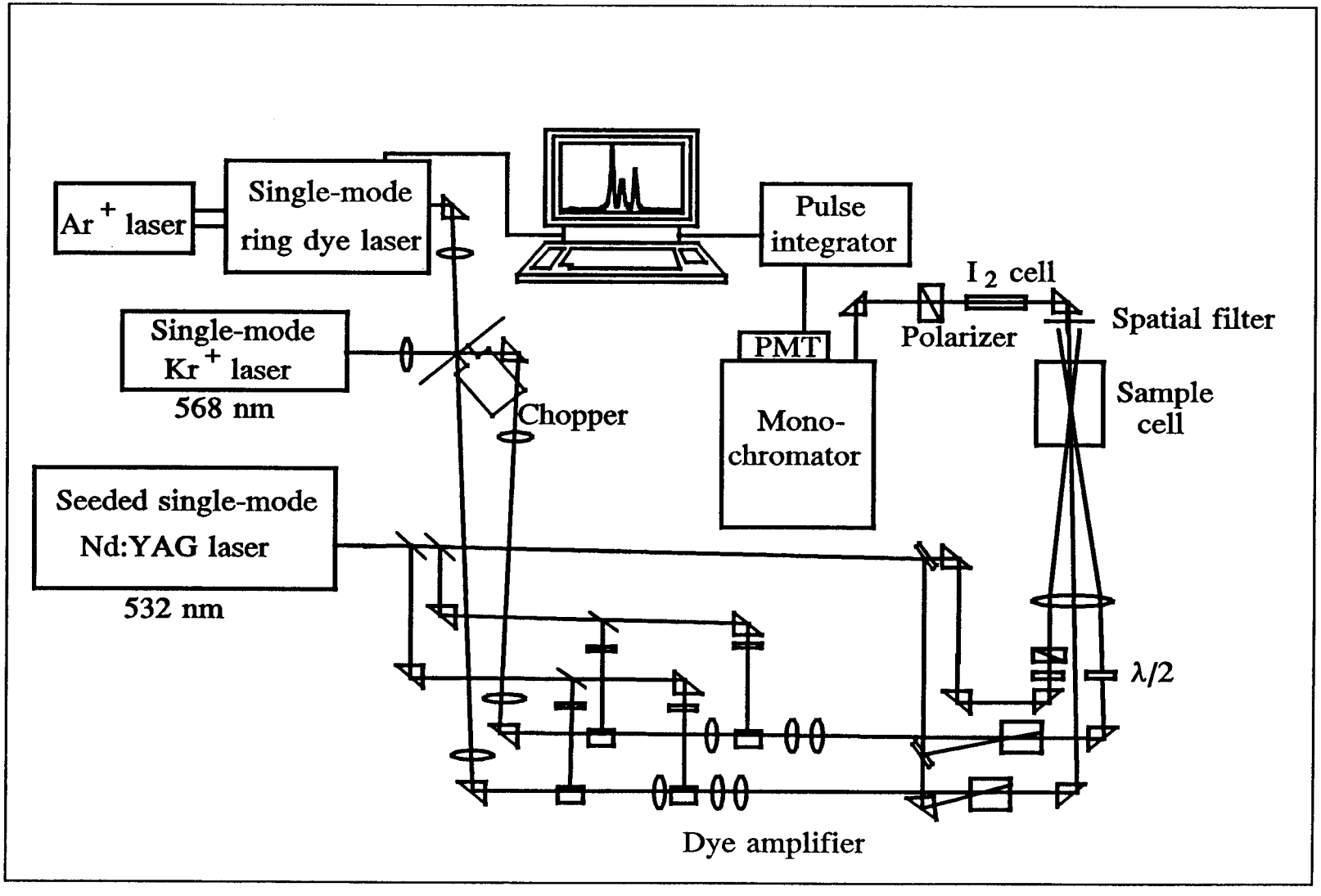

Figure II,3: High resolution CARS apparatus at OSU.

C: High Resolution Pure Rotational CARS Spectra of C_2H_6

The pure rotational CARS spectra of C_2H_6 were measured using the high resolution CARS apparatus described in the previous section. The S(J) lines of the ground state (all $v_i = 0$) and the S(J) lines of the molecules in the low-lying torsional state ($v_4 = 1$) were resolved for the first time. The rotational transition frequencies of each individual S(J) line of static C_2H_6 from J=10 to J=30 were measured at a pressure of about 200 Torr and room temperature. Figures II,4 - II,10 show CARS spectra for each line.

Because of the low value of I_A/I_B (~0.25) it is expected that the S branch will be much more intense than the $\Delta J = \pm 1$ R branch, which is also allowed[35]. A scan of two consecutive lines (S(22) and S(23) shown in figure II,11 shows no evidence of an R line where one is expected midway between the two S lines. In fact this scan served as strong support for the conclusion that the weak features are indeed the rotational lines of the low-lying torsional state ($v_4 = 1$), rather than R lines. Moreover, it can be seen from figures II,4 - II,10 that in some S lines there is a much weaker third line. Calculation of the R line positions indicates that these lines too do not belong to the R branch, and these lines are assigned as the

rotational lines of the second low-lying torsional state ($\upsilon_4 = 2$) at ~544 cm^{-1}. Unfortunately, the lines are very weak and the number of them observed was not enough to analyze to get accurate rotational constants as was done below for the other two states .

The spectra shown in figures II,4 - II,10 also suggest that there may be some kind of resolved K structure within each peak. However repeated scans, such as that of S(19) shown in figure II,13, shows that these peaks are not reproducible and are simply noise resulting from the highly nonlinear nature of the CARS process. In fact, the D_{JK} centrifugal distortion term in equation 3, which would produce K splittings within each J transition, is included in the simulation process discussed below where it is shown that such splitting should not be resolved under our experimental conditions.

Rotational constants

The first column of tables II,2 and II,3 gives the Raman shifts for the main band and the hot band, respectively. These values were obtained by measuring the CARS peak maxima and, in order to judge their accuracy, several factors which contribute to the uncertainty in our measurements must be considered.

First, the maximum of the CARS peak determination has been done using a peak-pick routine which is part of the dye laser software. This routine has been found to give a

reproducibility of about 0.004 cm^{-1} for peaks with our signal to noise ratio. Combining that with the uncertainty of the I_2 lines used in the calibration process (0.002)[37] gives an estimated frequency uncertainty of ±0.005 cm^{-1}.

Second, a CARS interference effect is expected to contribute to the uncertainty of values of neighboring lines. This effect has been noticed in other CARS studies and discussed in detail by Brown[37]. In summary, two adjacent lines can have a small frequency shift depending on the line width and the separation between the two lines. For small separations, the shifts are linear in separation and reach a maximum when the separation is ~0.5 times the line width, in which case the two peak maxima are shifted inward by ~0.25 times the line width. This maxima shift decreases as the separation increases and, because of the extended wings of the CARS peaks, the two peak maxima "push" each other away. This outward shift reaches a maximum when the separation of the two peaks is ~1.5 times the line width. This effect is noticed to be greater for the weaker of two interacting lines, as in the case at hand where the hot band lines are weaker than the main band lines. Therefore, a small negative correction of the order of few thousandths of a wavenumbers might be expected for the measured. Accordingly, small corrections were applied to the measured frequencies in an interative fit as will be discussed later.

The two sets of the measured and corrected frequencies of the main band and the hot band have been fitted to the well known equation

$$S(J) = (4B - 6D_J - 4D_{JK}K^2)(J + \frac{3}{2}) - 8D_J(J + \frac{3}{2})^3 \quad (II, 3)$$

Since no K structure was resolved, the D_{JK} term was taken to be zero. In the analysis, graphs of S(J) / 4(J+3/2) versus [3/2 + 2(J + 3/2)^2] were plotted , as shown in figures II,12 and II,13 for the main band and the hot band, respectively. The intercepts with the ordinate axis thus give the values of B and the slopes give the values of $-D_J$. The resulting values of B and D_J are listed in tables II,4 along with the recently reported values obtained from a high resolution infrared vibration rotation study[34]. The overall agreement is good and in the range of the uncertainty of our measurements.

Table II,2: Main band (υ_4=0) S rotational transitions (cm^{-1}).

J	ν (exp)	ν'= ν+Δ	ν(IR)-ν	ν(IR)-ν'
10	30.476	30.493	0.009	-0.007
11	33.137	33.147	-0.003	-0.013
12	35.785	35.794	-0.003	-0.012
13	38.437	38.445	-0.008	-0.016
14	41.080	41.087	-0.005	-0.012
15	43.722	43.727	-0.001	-0.006
16	46.368	46.373	-0.002	-0.007
17	49.013	49.027	-0.003	-0.017
18	51.648	51.650	0.005	0.003
19	54.294	54.295	0.001	0.001
20	56.931	56.934	0.005	0.002
21	59.580	59.583	-0.004	-0.007
22	62.218	62.221	-0.003	-0.006
23	64.856	64.856	-0.003	-0.003
24	67.487	67.492	0.002	-0.003
25	70.127	70.135	-0.002	-0.010
26	72.754	72.761	0.005	-0.003
27	75.385	75.395	0.006	-0.004
28	78.016	78.029	0.006	-0.007
29	80.647	80.657	0.005	-0.005
30	83.271	83.284	0.009	-0.004

Table II,3: Hot band (υ_4=1) S rotational transitions (cm^{-1}).

J	ν(exp)	ν' = ν+Δ	ν (IR)-ν	ν (IR)-ν'
11	33.004	33.019	0.004	-0.011
12	35.639	35.657	0.007	-0.012
13	38.282	38.301	0.000	-0.018
14	40.918	40.936	0.001	-0.017
15	43.542	43.560	0.012	-0.006
16	46.180	46.199	0.009	-0.010
17	48.817	48.841	0.006	-0.017
18	51.447	51.469	0.009	-0.013
19	54.080	54.093	0.009	-0.005
20	56.706	56.724	0.014	-0.005
21	59.341	59.356	0.009	-0.007
22	61.973	61.989	0.006	-0.010
24	67.227	67.248	0.006	-0.015
25	69.843	69.868	0.016	-0.010
26	72.471	72.494	0.011	-0.012
27	75.093	75.119	0.012	-0.014
28	77.712	77.741	0.015	-0.015
29	80.329	80.354	0.017	-0.008
30	82.957	82.987	0.008	-0.022

Table II,4: Rotational constants of C_2H_6.

State	parameter	this work cm^{-1}		literature[34] cm^{-1}
		observed	corrected	IR
$\upsilon_4 = 0$	B	0.663036(33)	0.663188(35)	0.6630279(28)
	$10^6 x D_J$	1.072(29)	1.130(30)	1.0324(23)
$\upsilon_4 = 1$	B	0.660384(28)	0.660691(34)	0.6604975(31)
	$10^6 x D_J$	1.031(21)	1.089(29)	1.0197(32)

As another form of comparison, the S(J) transitions were recalculated using equation 3 and the infrared rotational constants given in table II,4 . The infrared reported D_{JK} of 2.651 x 10^{-6} and 2.717 x 10^{-6} cm^{-1} for the main band and the hot band, respectively, were also included in the calculation. The third column of tables II,2 and II,3 gives the differences between the observed and the calculated transitions,and for the main band, we can see that these are generally with in the limits implied by the uncertainty of our measurements. However, asmall negative difference, which increases as J increases, does seem to be real for the hot band. This negative difference arises from the CARS interference effect mentioned earlier. An interative fitting procedure was done to reduce the discrepancies. Column four of tables II,2 and II,3 gives

the difference between the corrected and the IR calculated frequncies. Surprisingly, the agreement with the calculated frequencies was better for the observed data.

Spectral simulation

To reproduce the observed spectra of the S(J) lines, the transitions were first calculated using equation II,3 and the observed transitions analysis results listed in table II,4. The calculated transitions were then given a stick spectra using the line intensity equation

$$I_{JK}(CARS) = [g_{JK}\, b_{JK,\,J+2\,K}\, e^{-(F_{JK}-F_{J+2,K}/kT)}]^2. \quad (II,4)$$

Here $b_{JK,J+2\,K}$ is given by[35]

$$b_{JK,J+2\,K} = \frac{3[(J+1)^2 - K^2][(J+2)^2 - 2)^2 - K^2]}{2(J+1)\ (J+2)\ (2J+1)\ (2J+3)} \quad (II,5)$$

and g_{JK} is given by

$$g_{JK} = 2g_{ns,JK}\ (2J+1) \quad (II,6)$$

and should be divided by 2 when K = 0. g_{ns} is the nuclear spin statistical weight which has been calculated using the same procedure described in chapter I and found to be

K = 0	J = even	g_{ns} = 8
K = 0	J = odd	= 16
K = 3p		= 24
K = 3p±1		= 20

The relative population of the torsional state has been determined by the Boltzmann distribution relation. About

25% of the molecules are in this state at room temperature, which gives the hot band a CARS intensity of 6.25% of the main band intensity. However, the hot band was noticed to have slightly higher relative peak intensity. Examining the line widths and the areas of the two bands showed that the line width (FWHM) of the hot band was smaller than that of the main band. The peak area of the hot band was also measured and found to be 7-10% of that of the main band, which is in consistant with the predicted relative peak intensity. The higher line width of the main band causes the peaks to broaden and hence bring the peak maxima down. In the hot band, the sharper lines stand out more strongly and hence have enhanced relative intensity. Why the hot band lines should be sharper is not known but presumably results from reduced effectiveness of collisional relaxation.

After producing the stick spectrum, the various line broadening contributions were considered. The natural line width is expected to be extremely small so that collisional, Doppler, and instrumental broadening will dominate. The Doppler effect was calculated taking the crossed beam geometry into consideration, in which case the Doppler FWHM is given by[35]

$$\Delta\nu = \Delta\nu_{DOP}\,[1+4\sin^2\frac{\theta}{2}\,(\nu_o+\nu_o\nu_R)/\nu_R^2]^{\frac{1}{2}} \qquad \text{(II,7)}$$

where $\Delta\nu_{DOP}$ is the Doppler width for collinear beams, ν_o is

the laser frequency, ν_R is the rotational transition and θ is the crossing angle of the two yellow beams (~1.95°). Using this equation, the Doppler width has been found to be of the order of 0.001 cm^{-1}. The instrumental width of the system used is known to be 0.005 cm^{-1}, however a previous CARS studies showed that an increase of a factor of 2 is expected because of power saturation and AC stark effects. Because the experiment was done at high pressure (~200 Torr), the collisional broadening is expected to be the highest of all. In fact, during the simulation process $\Delta\nu_{COL}$ has been found to be about 0.07 cm^{-1}.

In the simulation process, the stick spectrum was first given a Lorentzian line shape to account for the collisional broadening. Then a Gaussian function was convoluted over both the real and imaginary parts of the Lorentzian lineshapes to account for the Doppler effect. Finally, the two parts of χ were squared, added and convoluted by the Gaussian laser lineshape function using a Fourier transform method.

Since each S(J) line transition was measured separately, the process was done first on each line separately. An interative fitting was done by repeating the process making small changes in the collision broadening line width and the stick spectra positions of the two bands until the observed CARS spectrum was reproduced. The magnitude of the corrections needed to

repreduced the observed spectra as a function of J are shown in figure II,14. These frequencies shifts resemble the CARS interference effect discussed earlier. Figure II,15 shows the simulated spectra of S(15) and S(25) where the good quality of the fit can be seen.

The simulation process was then repeated over the whole region from S(10) to S(30) using the parameters $\Delta\nu_{COL} = 0.07$ and $\Delta\nu_{DOP} = 0.001$ cm^{-1}, which are the avarage of the parameters that gave the best fit of individual S lines. The final result is shown in figure II,16. It can be noticed that the relative intensities are not the same for the calculated and observed bands. The reason is that the lines were measured individually, and the relative intensities among different values of J were not considered during the experiment.

In general, the spectra are in excellent accord with those predicted from the very accurate vibrational-rotational data. The results also show no evidence of spectral torsional splittings or shifts, as one would predict from the small magnitude of torsional effects for low lying torsional levels.

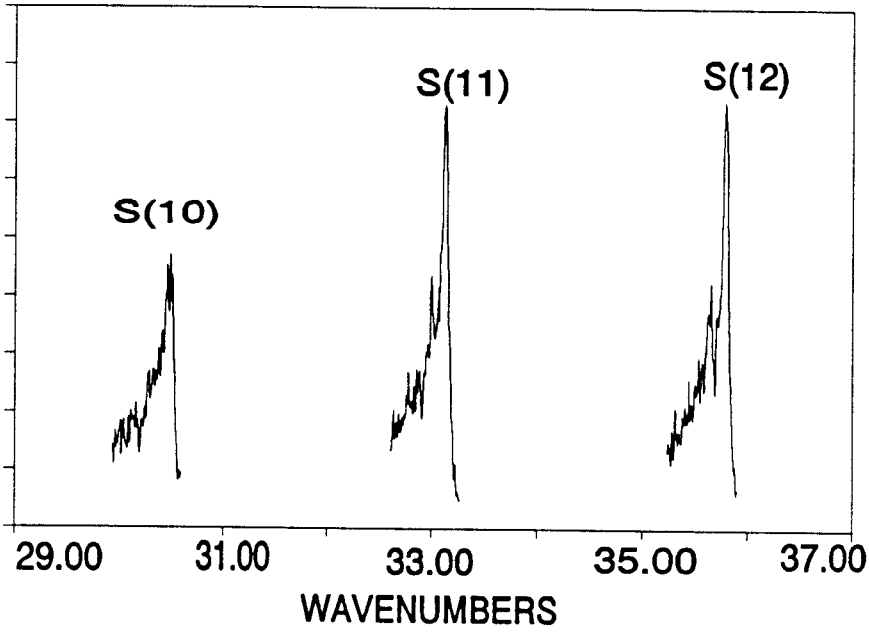

Figure II,4: S(10), S(11),and S(12) of C_2H_6 at 200 Torr and 300 K.

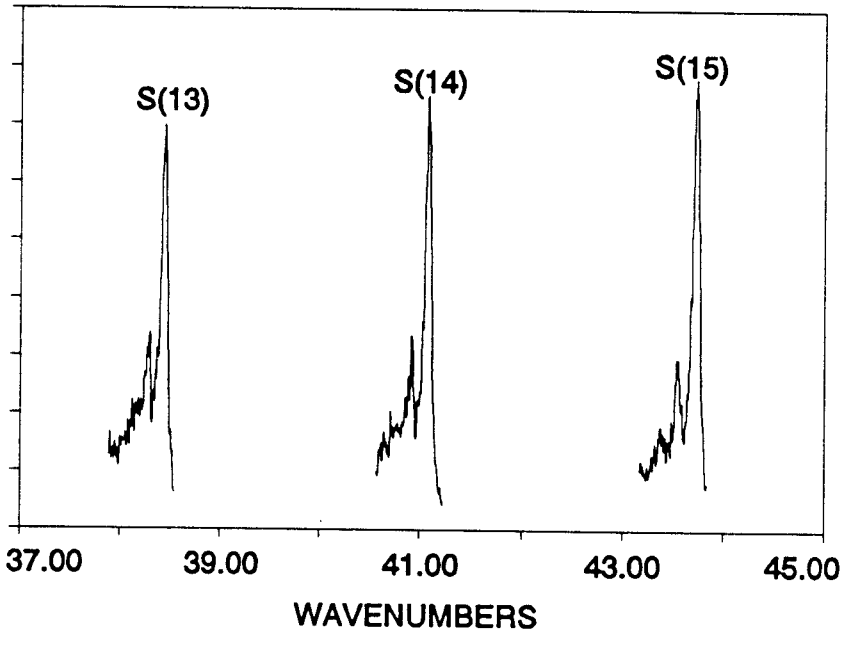

Figure II,5: S(13), S(14), and S(15) lines of C_2H_6 at 200 Torr and 300 K.

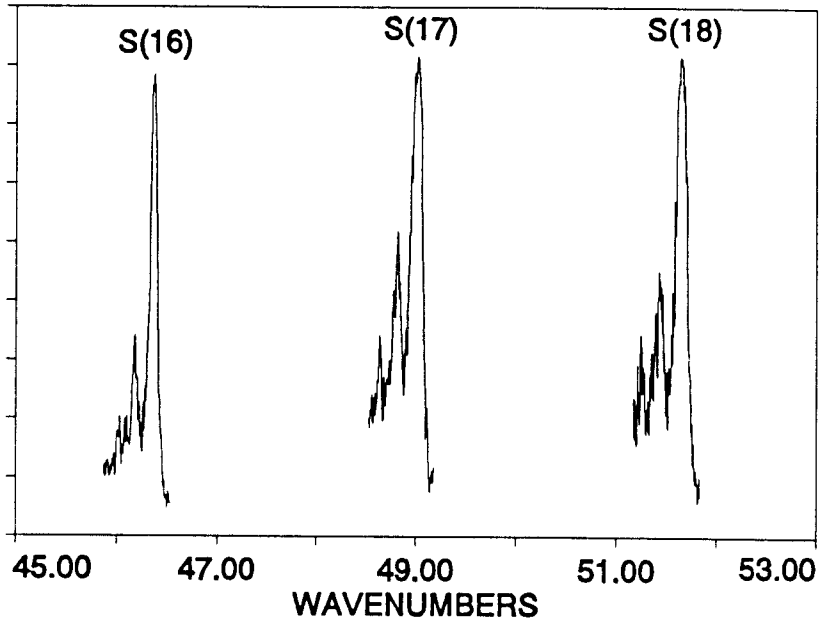

Figure II,6: S(16), S(17), and S(18) lines of C_2H_6 at 200 Torr and 300 K.

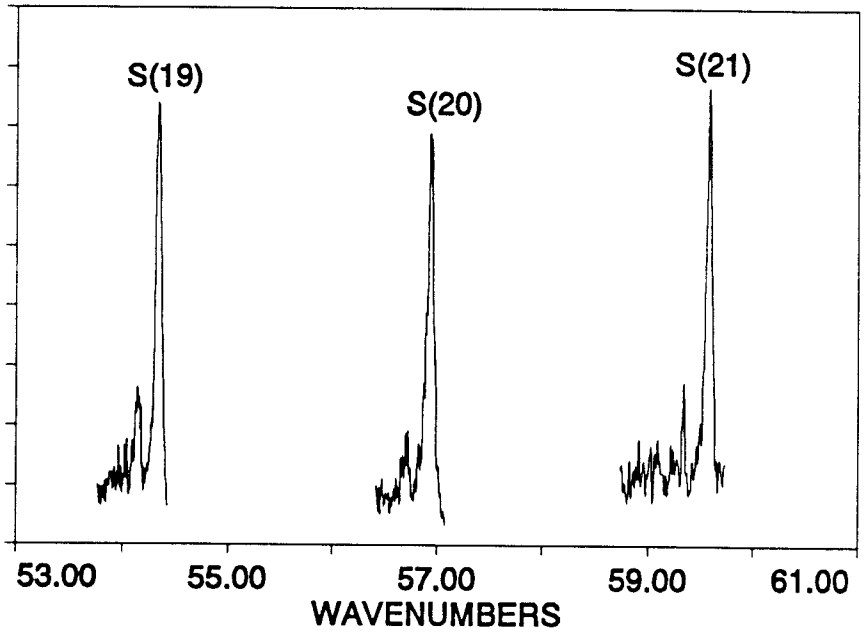

Figure II,7: S(19), S(20), and S(21) lines of C_2H_6 at 200 Torr and 300 K.

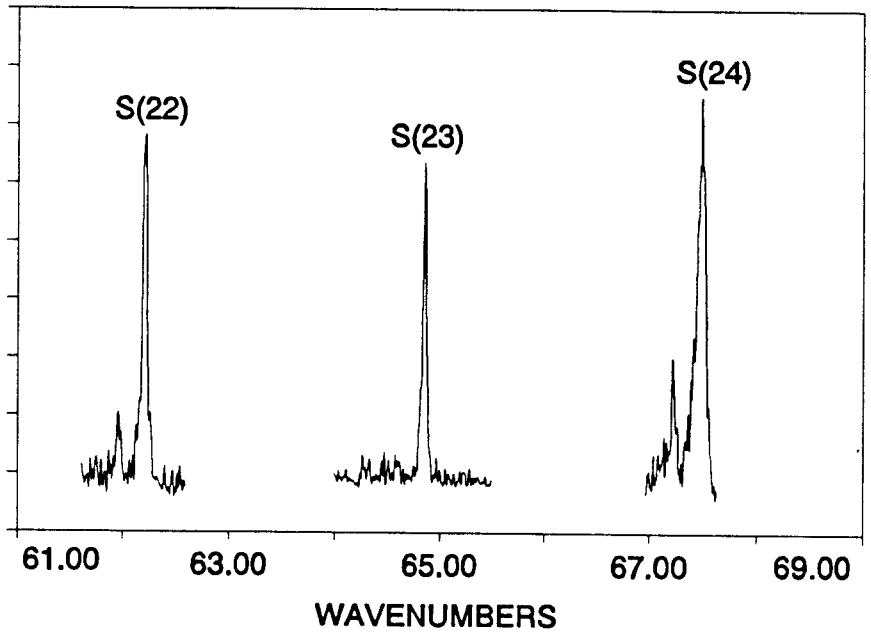

Figure II,8: S(22), S(23), and S(24) lines of C_2H_6 at 200 Torr and 300 K.

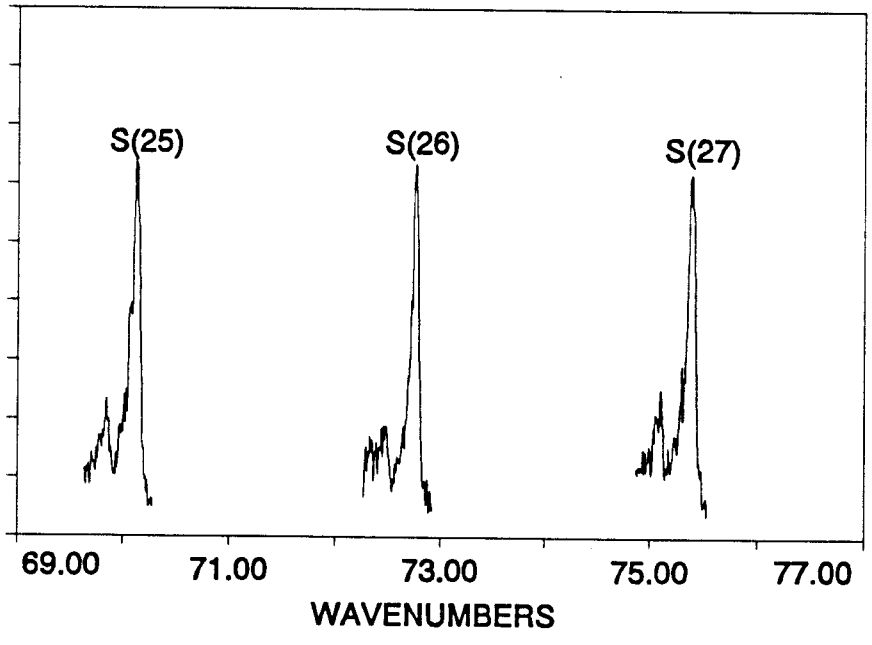

Figure II,9: S(25), S(26), and S(27) lines of C_2H_6 at 200 Torr and 300 K.

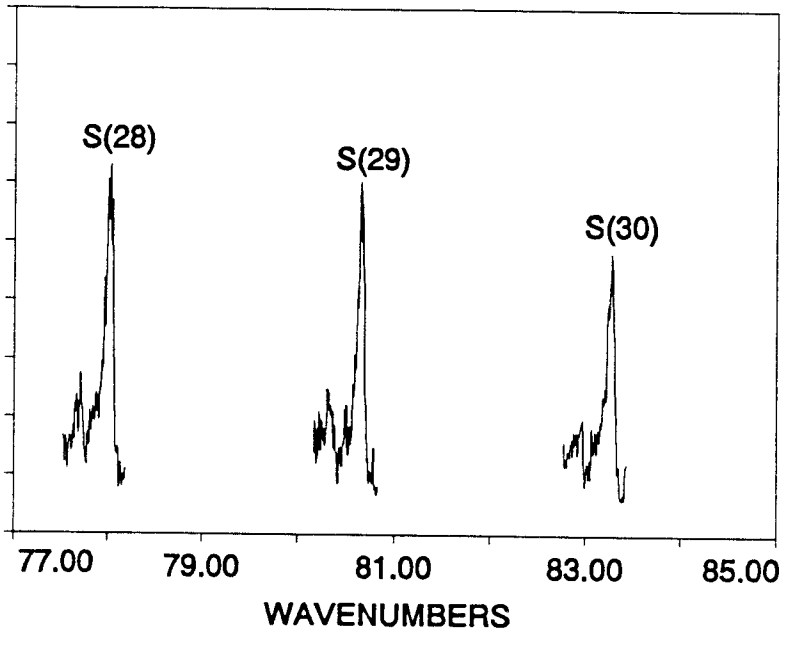

Figure II,10: S(28), S(29), and S(30) lines of C_2H_6 at 200 Torr and 300 K.

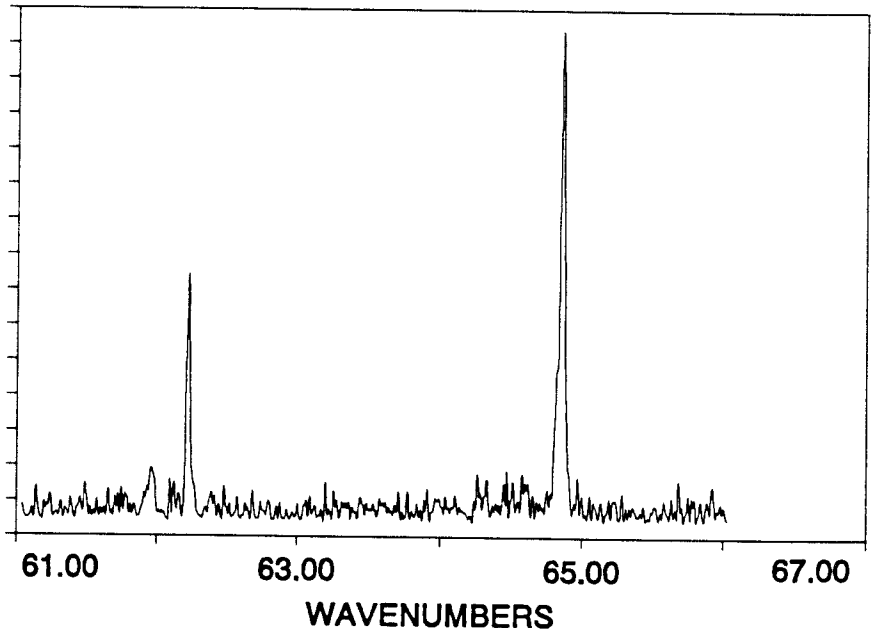

Figure II,11: S(22) and S(23) measured under one scan. There is no R line between the two lines where one is expected.

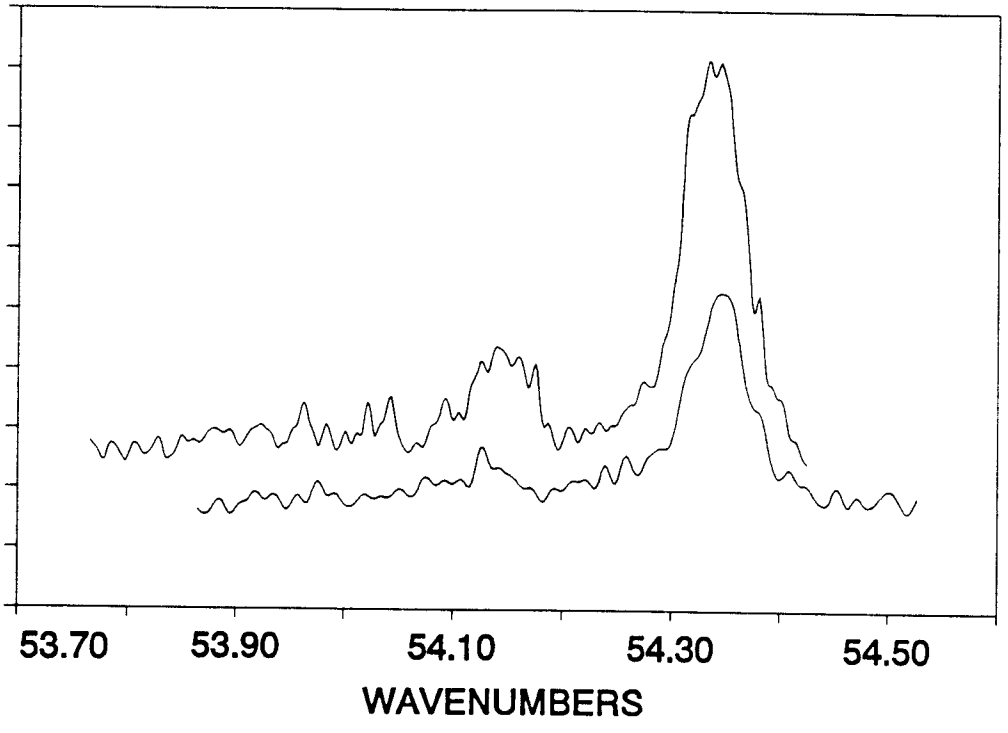

Figure II,12: A repeated scan of S(19) shows that the fine structure of the peaks is noise.

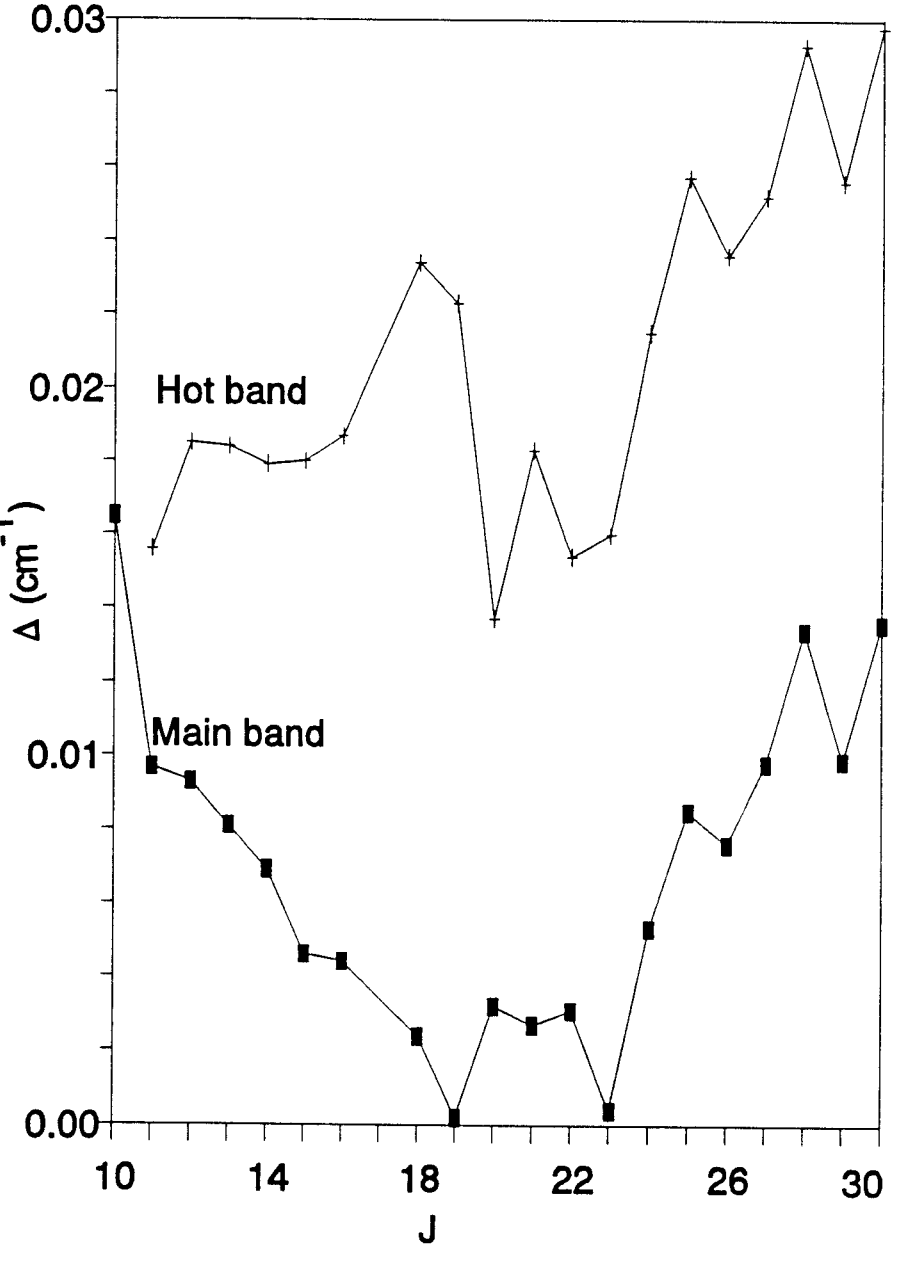

Figure II,13: The frequency shifts needed to reproduce the observed spectra as a function of J.

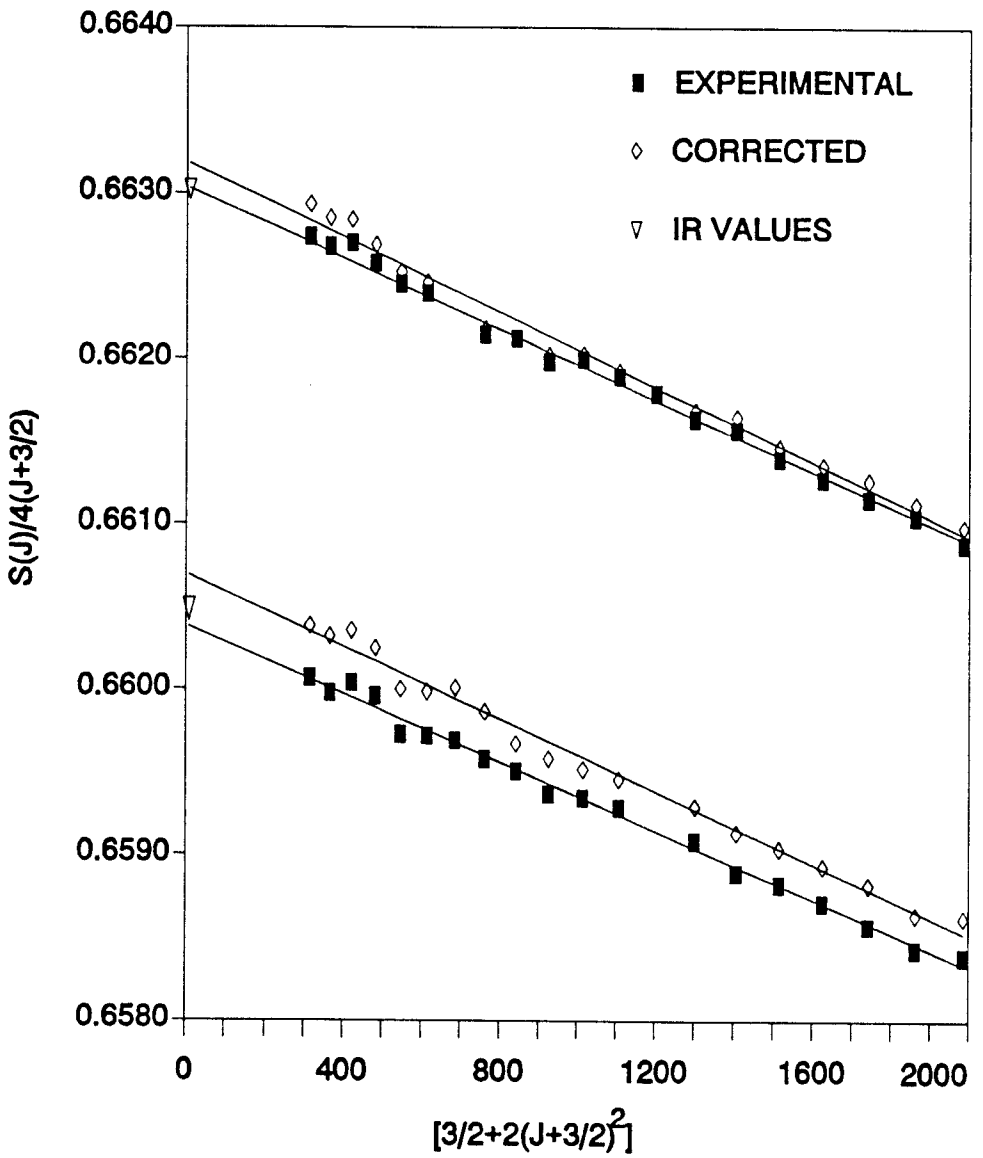

Figure II,14: Data analysis of the main band (upper) and the hot band (lower).

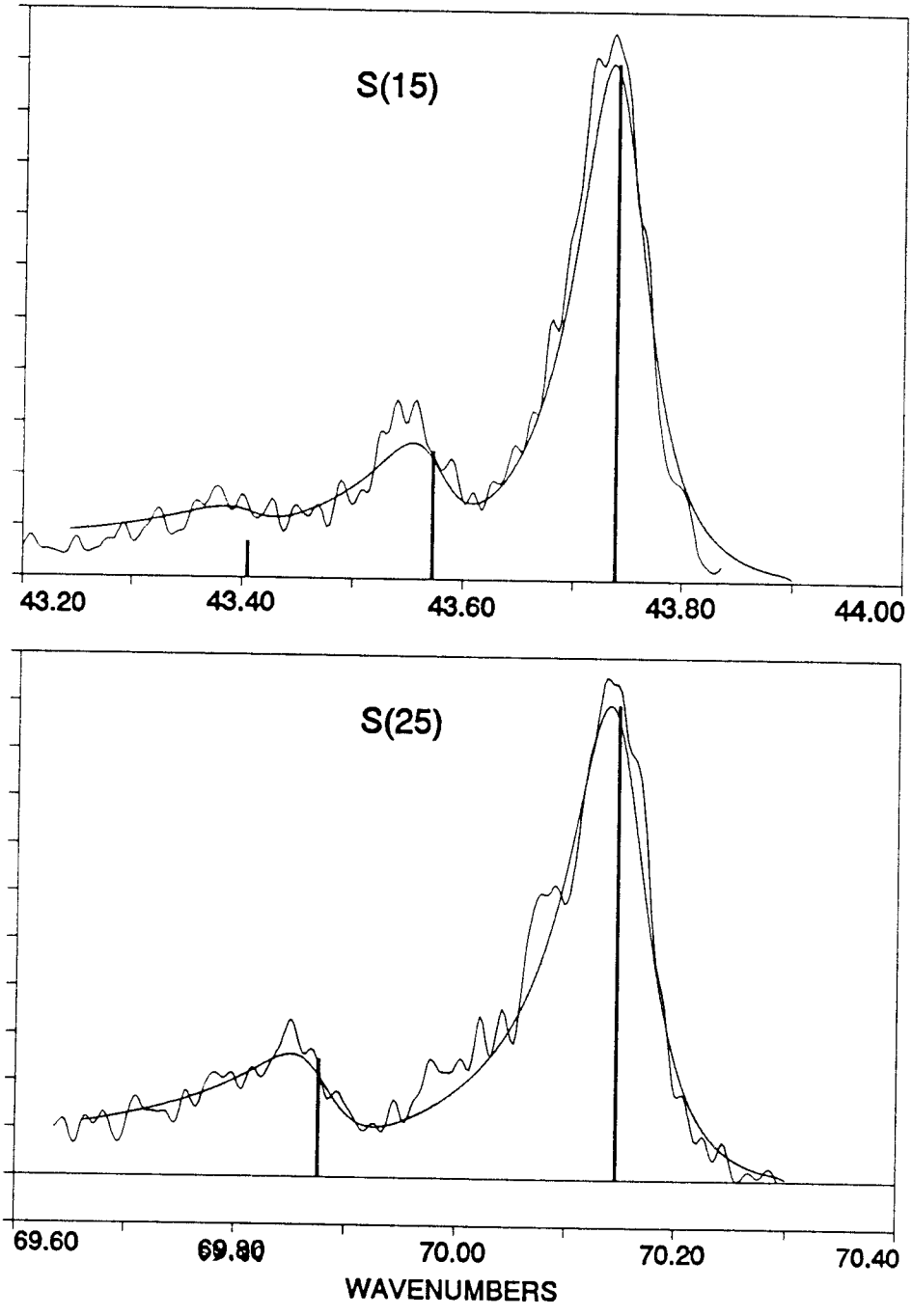

Figure II,15: Simulated spectra for S(15) and S(25).

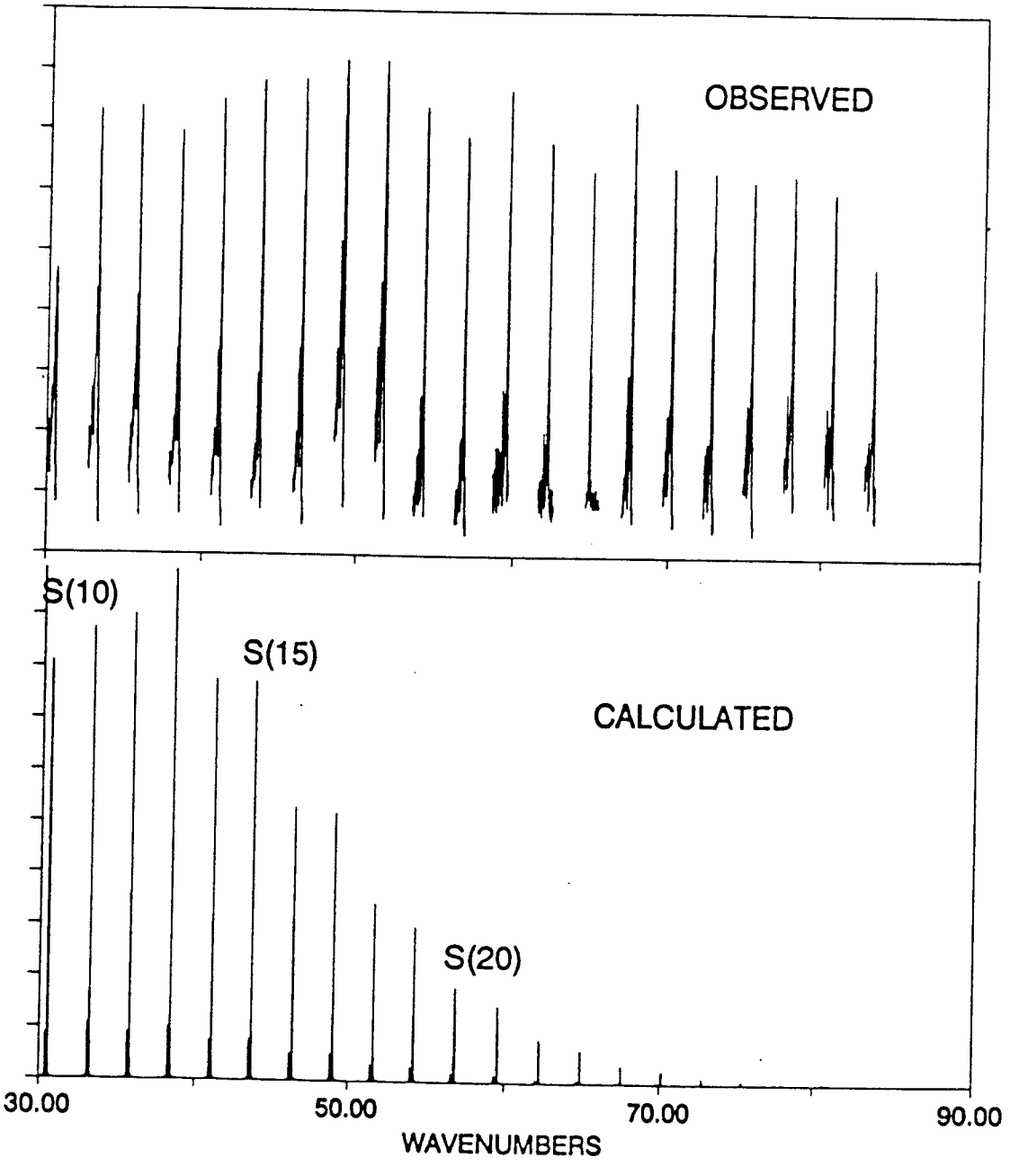

Figure II,16: Simulated spectrum for S(10) to S(30).

D: Vibrational-Rotational CARS Study Of the ν_3 Region

In this section, we report the results of a vibrational-rotational study of C_2H_6 by CARS. The high resolution of of our instrument allowed the first observation of individual J,K Q-branch transitions of ν_3, the totally symmetric C-C stretching vibration. This work was motivated in part by an interest in the possible discernment of small spectral splittings due to tunneling through the torsional barrier. A second question was whether the complex spectrum in this spectral region was due to more than one vibrational Q-branch and, if so, why.

The ν_3 region (900-1100 cm^{-1}) has been the subject of two Raman studies in the past. In the first[36], the ν_3 band origin was obtained by analyzing the resolved O and S branches ($\Delta J = 0$, $\Delta K = \pm 2$) accompanying the strong unresolved Q branch excited by a Hg 4358 line. ν_o = 994.75 cm^{-1} was reported as the ν_3 band origin. In the second study[33], the measurement of ν_3 was repeated in both static cell and free jet expansion experiments. Because of the low resolution (~2 cm^{-1}) the Q branch was not resolved in either experiment. From a simulation calculation, a value of 992.9 cm^{-1} was deduced as the band origin by the second group. No hot bands involving the torsion (ν_4) were resolved for ν_3 although they have been seen for other

vibrations.

In this work, the high resolution CARS apparatus described in section A was employed to measure resolved Q branch spectra of C_2H_6 in the 900-1000 cm^{-1} frequency range. Many of the J, K Q-branch lines have been measured and analyzed to give more accurate and new vibrational rotational parameters for the transitions involved. Spectra were recorded for both static cell and free jet expansion conditions.

For the jet expansion experiments, the cell was evacuated continuously and the jet valve was pulsed synchronously with the laser. A nozzle diameter (D) of 250 μm was used and the sample was probed in different positions (X) downstream in the jet (X/D = 1 to 12). In some experiments, seeding the sample with He was done to get greater cooling of the sample. Different mixtures (50%, 25% and 12%) of C_2H_6 in He were used. Also tried were different driving pressures (P0 = 15 to 200 PSI) for both neat and seeded ethane.

At the end of this work, several experiments were done with a new Nd-YAG laser source (Continuum-custom long pulse model) just arrived in our lab. The resolution of this source is improved by a factor of 10 (0.0005 instead of 0.005 cm^{-1}). For the collisional width at the sample densities used however, the results of the two systems are

almost identical, i.e. no more lines were resolved using the higher instrumental resolution.

Results

In addition to the ν_3 fundamental, several other bands might be expected to be seen in the frequency range of study. Indeed the ν_4=n + ν_3=1 ← ν_4=n + ν_3=0 sequence with n= 0, 1, and perhaps 2 could be anticipated since ν_4=289 cm^{-1} is low enough for appreciable population of the n = 1 (25%) and 2 (7.3%) levels. In addition, although it has not been confirmed by experiment, some calculations predict that the $4\nu_4$ overtone transitions are expected in this range too[33] and these might mix with ν_3 and gain intensity due to a Fermi resonance interaction.

Figure II,17 shows the CARS Q-branch of C_2H_6 in the totally symmetric stretching vibration region. Trace a was obtained in a static cell with neat C_2H_6 at 34 Torr. As can be seen, this spectrum is exceedingly "rich" and very hard to analyze the way it is. It might well be that more than one band is involved, although it is not easy to see any obvious band origins except perhaps the one around 995 cm^{-1}. Thus cooling of the sample was highly desirable to simplify the spectrum.

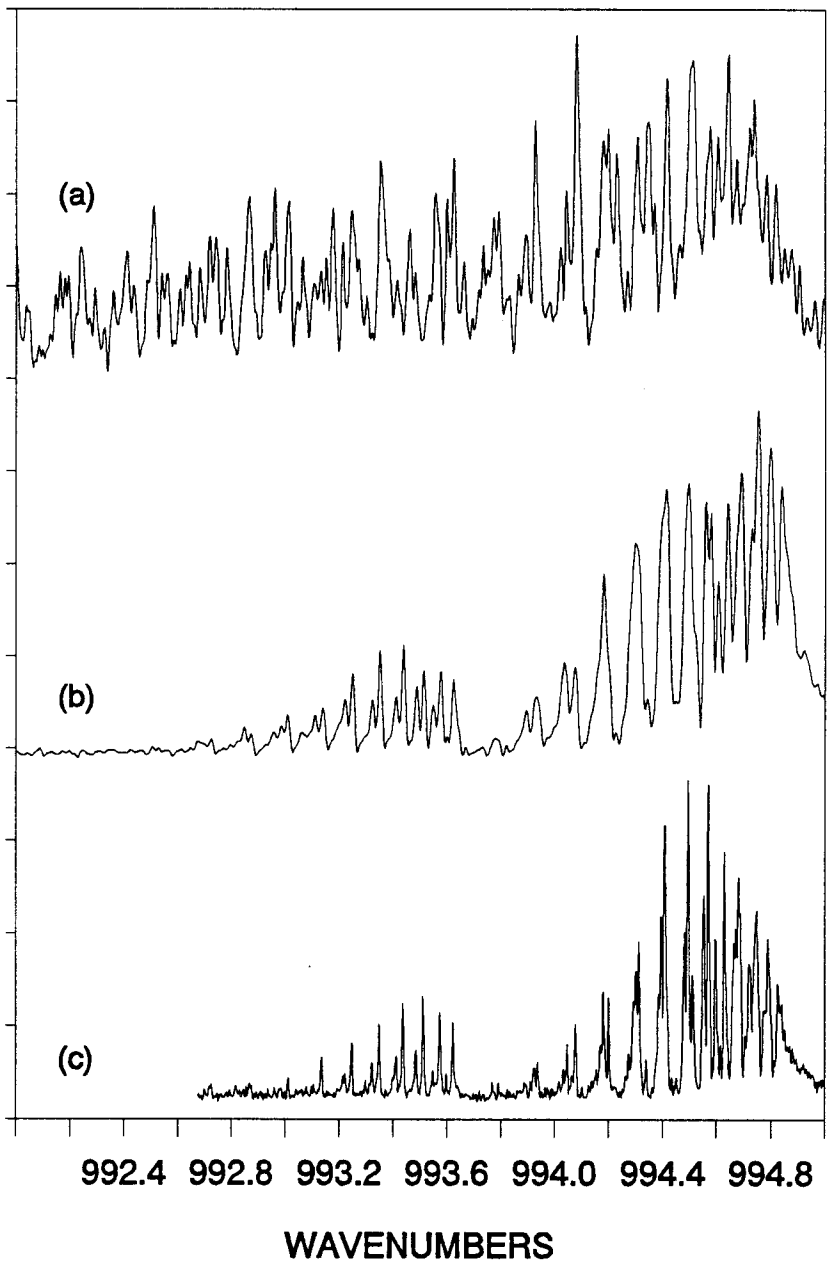

Figure II,17: Spectra of C_2H_6 in a static cell at 300 K and 34 Torr (a), in a free jet expansion of neat C_2H_6 at X/D=7 (b), and in a free jet expansion of a 50% mixture of C_2H_6 in He (c).

Trace b is the spectrum of neat C_2H_6 recorded in a free jet expansion at X/D = 7 and a driving pressure of 2.4 atm. Comparison with the static cell spectrum at room temperature (a), shows that the cooling of ethane in the jet resulted in a much simpler spectrum, with two clearly different band progressions. The weaker low frequency band sequence is fairly clean, and suggests that analysis shuld be possible. The high frequency band, however, is still complex, suggesting that further cooling of the sample was desirable. As can be seen, many lines are still overlapped resulting in perturbation of the CARS line intensities which made the assignments uncertain. Probing at larger X/D positions in the jet, where greater cooling is expected, along with varying the driving pressure, and seeding the sample with He carrier gas was thus required to achieve sufficient cooling of the sample to allow a confident interpretation of the spectrum.

Trace c is the spectrum of a 50% mixture of C_2H_6 in He measured in a free jet expansion at X/D = 6 and driving pressure of 4.4 atm. Comparison with traces a and b shows that seeding the sample with a monatomic collision partner gas such as He resulted in a simpler, sharper, spectrum. The latter two spectra thus were used in the analysis as discussed later. It should be mentioned that the three spectra shown in figure II,17 are representative of many

scans that were taken of both neat and seeded C_2H_6 and that the frequencies used in the analysis were obtained as averages of two to five measurements.

Spectral analysis

Possible role of torsional hot band.

From the relative intensities of the two bands, we first considered the possibility that the high frequency band the fundamental transition ν_3=1, ν_4=0 ← ν_3=0, ν_4=0, with the low frequency band due to the hot band transition ν_3=1, ν_4=1 ← ν_3=0, ν_4=1. That such a vibrationally hot band could be seen in the jet is not unreasonable since it is known that vibrational cooling can be less effective than rotational cooling in free jet expansions.

However, when analyzing the spectrum using this assumption, we ran into several problems. First, the rotational parameter differencies resulting from the analysis were unreasonably high. Second, figure II,17 shows a sudden intensity drop at the band head region which could not be reproduced for any hot band assignment. Third, the variation of the spectra with temperature showed that the high frequency band could not be attributed to one band system. Figure II,17 shows that, with cooling, a dramatic intensity decrease seems to occur at the high frequency, band head region. This is a

startling result at the low J,K converging band head position since cooling is expected to build up intensity here. After some considerable effort to try to fit this high frequency band in a single sequence, we have been unsuccessful and have reached the conclusion that this band consist of more than one Q branch. However,it seemed to be clear that the extra Q band(s) could not be due to torsional hot bands since the intensities was much too high. In addition, consideration of all other hot bands for C_2H_6 shows that they would occur well above the 1000 cm^{-1} region and would have low intensity.

The final compelling evidence that torsional hot bands need not be considered comes from the jet studies of Stolte et al[33]. Although their resolution was insufficient to see the ν_3 structure of interest, they did study other bands where torsional hot bands were observed to disappear on cooling in a jet. A similar observation was done by Owying et al[43] in a jet study of the complix ν_1 region of C_2H_6. Thus efficient collisional depopulation of the higher torsional levels seems to occur in these expansions.

Possible role of torsional sub levels.

The elimination of hot band contributions leives then the possibility that the extra Q bands in the ν_3 region are due to torsional splittings. In particular, detailed

theoretical arguments[30] using the full G_{36}^{+} group appropriate to the torsional problem shows that every vibrational state of C_2H_6 consists of 6 sublevels which are generally degenerate except for the higher torsional levels. Each torsional sublevel below the top of the torsional barrier is characterized by its symmetry species, which is A_{1s}, E_{3d}, E_{3s} and A_{3d} for even values of υ_4 as is the case for the ground state and $4\nu_4$. Teory predicts that these sublevels occur at splitting energies of -2S, -S, S and 2S, respectively, and that the splitting parameter (S) increases dramatically within each grouping of four as υ_4 increases.

To analyze the spectrum, it is necessary to know the vibration-rotation-torsion species of each J,K level, which can be formed as the direct product of the vibration, rotation and torsion species. For totally symmetric states such as ν_3 and $4\nu_4$ the vibrational symmetry species is A_{1s}. The species of the rotational functions depend only on the quantum number K and exhibit a periodicity of 6; For K=1, 2, 3, 4, 5, and 6 the species are E_{2d}, E_{1s}, $E_{3d}+A_{4s}$, E_{1s}, E_{2d}, and $A_{1s}+A_{2s}$, respectively. For K=0 the species are A_{1s} for J even and A_{2s} for J odd. Using this procedure it results that A_{1s} and E_{3s} torsional sublevels exist only for even values of K while A_{3d} and E_{3d} torsional sublevels exist only for odd

values of $K^{(30)}$. Moreover, each one of these sublevels has nuclear spin statistical weights which are found by taking direct products of the vibration-rotation-torsion species of each sublevel and the nuclear spin species [which are $10A_{1s}+6A_{4s}+3E_{1s}+E_{2s}+E_{3s}+E_{4s}+8G^{(30)}$]. The total symmetry must be A_{2d} or A_{1s} to yield a sign change on exchanging of any two protons[30]. Table II,5 summarizes the results of the calculations using the above procedure. In table II,5, are given the allowed values of K and the nuclear spin species whose weihting coefficient can be added to get the total nuclear spin statistical weight for each sublevel.

Such symmetry predictions agree well with the results of measurements of the high ν_4 torsional states. However it should be noticed that the splittings (S) among these torsional sublevels will be small for transitions in which ν_4 is unchanged. For example, for the ν_9 mode at 822 cm^{-1},

Table II,5: Nuclear spin species, statistical weight and allowed values of K for the four torsional state sublevels.

	A_{1s}	E_{3d}	E_{3s}	A_{3d}
K=0 J even	$6A_{4s}$		$2E_{4s}$	
K=0 J odd	$10\ A_{1s}$		$6E_{3s}$	
K=1,3,5,..		$16G_s$		$3E_{1s}+E_{2s}$
K=2,4,8,..	$E_{2s}+3E_{1s}$		$16G_s$	
K=3,9,15,..		$2E_{4s}+6E_{3s}$		$6A_{4s}+10A_{1s}$
K=6,12,18,..	$6A_{4s}+10A_{1s}$		$2E_{4s}+6E_{3s}$	

the splittings of the upper level are less than 0.005 cm^{-1} and those for the ν_3 should be comparable or smaller. Thus our observation of at least two Q-branch bands separated by about 1 cm^{-1} is strong evidence that the structure is not simply due to a large splitting parameters (S).

Possible role of Fermi resonance.

This leaves then the interesting possibility that the complexity of the ν_3 spectrum may due to Fermi resonance interaction with an overtone transition of A_{1g} symmetry. That such interacion mighrt occur between $4\nu_4$ and ν_3 has infact been predicted by several groups but no experimental confirmation has been found.

The calculations of reference (33) predict A_{1s}, E_{3d}, E_{3s}, andA_{3d} sublevels of $4\nu_4$ to be at 875.56, 899.71, 951.77 and 1005.65 cm^{-1}, respectively. Figure II,18, taken from (33) shows the predicted Fermi resonance interactions that could occur between different overtones of ν_4 and ν_3.

In a Fermi resonance interaction, it is well known that only vibrational levels of the same species can perturb one another. Moreover, the magnitude of the shift induced by such interaction depends on the separation between the two interacting levels[17]. The smaller the

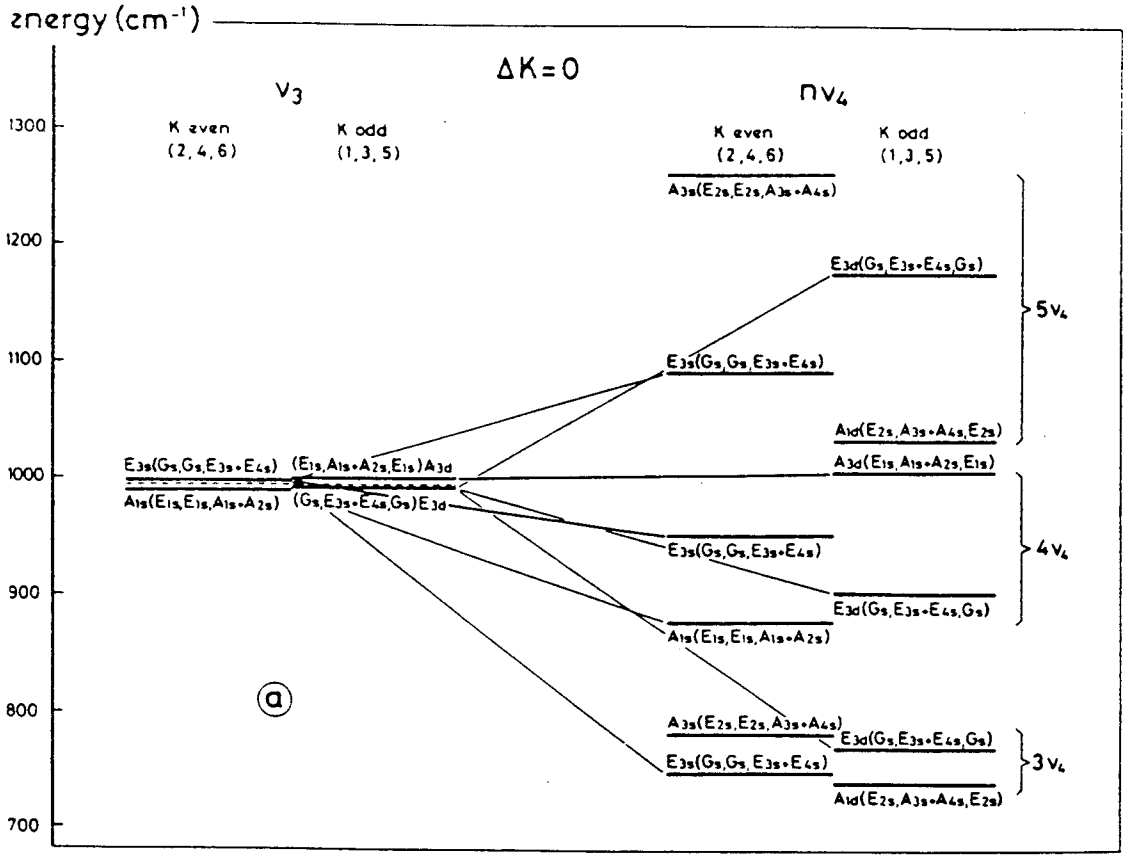

Figure II,18: Possible Fermi Resonance interaction between the ν_3 fundamental and the ν_4 overtones. Taken from reference(33).

separation the greater the shift from the mean of the unperturbed levels. It can thus be seen that $4\nu_4$ sublevels are the most likely candidates for a vibrational mixing with their ν_3 counterparts.

Comparing the observed spectrum and the positions of $4\nu_4$ torsional sublevels (given above and shown in figure II,18), one would expect the A_{3d} torsional sublevel of ν_3 to have the greatest shift, and to lower frequency. The other three sublevels will have smaller shifts to higher frequencies. The ordering of the shift will thus be $E_{3s}>E_{3d}>A_{1s}>\nu_3$ origin$>A_{3d}$. Using this assumption the observed spectrum has been analyzed as discussed below.

Assignments

The Q-branch rotational analysis of the spectrum is based on the fact that C_2H_6 is a prolate symmetric top, for which the rotational energy levels of a given vibrational state are given by

$$F_v(J,K) = BJ(J+1) + (A - B)K^2 - D_J J^2(J+1)^2 - D_{JK} J(J+1)K^2 - D_K K^4 \qquad (II,8)$$

The selection rules for the Q-branch of a totally symmetric Raman active vibrational mode of the ν_3 type are $\Delta J = 0$ and $\Delta K = 0$, yielding Q-branch transitions at

$$Q(J,K) = (B'-B'')J(J+1) + [(A'-B') - (A''-B'')]K^2 - (D_J'-D_J'')J^2(J+1)^2 - (D_{JK}'-D_{JK}'')J(J+1)K^2$$

$$- (D_k'-D_k'')K^4 \qquad (II,9)$$

The assignment was first done for the low frequency band using trace c of figure II,17, which suggested a simple progression in J with some K structure. This band has been assigned to the A_{3d} torsional sublevel of ν_3. This assignment is supported by more than one piece of evidence. First, A_{3d} torsional sublevel consist only of odd K with statistical weights of 4 for K=1, 5, 7, ..., and 16 for K=3, 9,15,... as can be seen in table II,5. At low temperatures, therefore, one would expect a simple progression in J with some K structure corresponding mainly to K=1, and 3 with K=3 having enhanced peak relative intensity because of the higher statistical weight. Second, this assignment is supported by the sudden drop in the intensity at the band head region since the first strong line in the band would be J=3, K=3 which has much higher intensity than K=1 of J=1, J=2, or J=3 line.

In the analysis, an iterative assignment of the strong lines in the A_{3d} band region was done and the assigned lines were fit by linear regression to equation II,9. As the assignment became more certain by comparison of the difference between observed and calculated frequencies, more lines were added to the least squares set and the process was repeated until most of the lines

in the A_{3d} band region were accounted for. Table II,6 gives the measured frequencies for A_{3d} level obtained as averages of three different experimental measurements. Those marked with (*) were used in the fit. The assignments and simulated spectrum, which will be discussed later, are shown in figure II,19.

In the analysis of the high frequency band the assumption was made that the band contains all the Q-branch transitions of the other three torsional sublevels. The results of the A_{3d} band analysis then may aid in the analysis of that band since, to a good approximation, the different sublevels should have the same rotational parameters. On this basis the results of the A_{3d} band analysis were used in the following way.

The rotational parameter differences resulted from the analysis of A_{3d} band was used to calculat the Q-branch transitions. Three estimated shifts for the different high frequency sublevels were then added to the A_{3d} band origin. An iterative simulation of the spectrum similar to that discussed below was then performed making small changes in the shift of each component until the observed spectrum was reproduced. It turns out that most of the lines in the high frequency band region were severely overlapped which made the assignment somewhat

Table II,6: The Q-branch frequencies of the A_{3d} component of ν_3 (cm^{-1})

J	K	calc.	obs.	obs-calc
1	1	993.602	993.614	0.012
2	1	993.578	993.587	0.010
3*	3	993.564	993.568	0.004
3*	1	993.540	993.541	0.001
4*	3	993.514	993.518	0.004
4*	1	993.491	993.491	0.000
5*	3	993.452	993.456	0.004
5*	1	993.429	993.429	0.000
7*	7	993.408	993.405	-0.003
6*	3	993.378	993.381	0.003
6*	1	993.354	993.354	0.000
7*	5	993.338	993.337	-0.001
7*	3	993.291	993.294	0.003
7*	1	993.267	993.267	0.000
8*	5	993.238	993.240	0.002
8*	3	993.191	993.193	0.001
8*	1	993.168	993.163	-0.005
9*	3	993.079	993.081	0.002
9*	1	993.056	993.054	-0.002
10*	5	993.002	993.002	0.000
10*	3	992.955	992.954	-0.002
10*	1	992.932	992.926	-0.005
11*	3	992.819	992.814	-0.005
11*	1	992.795	992.792	-0.003
12*	3	992.670	992.671	0.001
12	1	992.646	992.637	-0.009

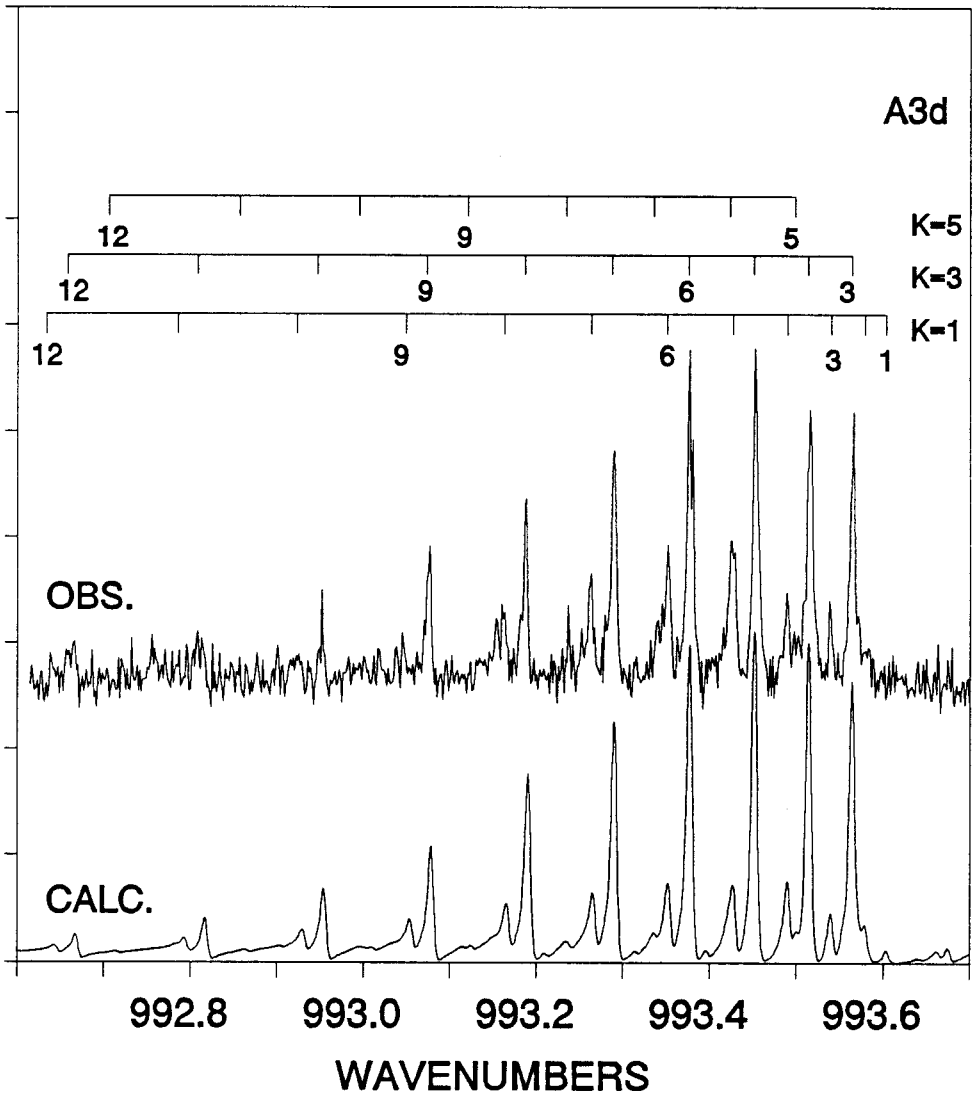

Figure II,19: Assignments and simulated spectrum for A_{3d} torsional sublevel of ν_3.

challenging. However, a number of the isolated lines were confidently assigned to the three different torsional sublevels and then compined with the A_{3d} lines for a simultaneous fit of all four sublevels. For this equation II,9 was used with the addition of three additional band origins for the three high frequency sublevels.

It should be mentioned here that the centrifugal distortion difference parameters were not included in the final fit. Including these parameters did not significantly reduce the obs-calc. frequency differences and the resulted parameters had large standard errors. Such high uncertainties might be expected since several parameters depend on K which has limited range in the spectra of cold C_2H_6 in the jet. Tables II,6 to II,9 show the observed, calculated, and observed-calculated differencies for A_{3d}, E_{3s}, A_{1s}, and E_{3d}, respectively. In these tables the frequencies that are marked with (*) are the ones that are used in the final fit.

Column five of tables II,6 to II,9 gives the difference between the observed and calculated frequencies. In general, the small magnitude of these differences can be taken as good support for the correctness of the assignments.

The top part of table II,10 gives the band origins of the torsional components of ν_3. Also given in the bottom

Table II,7: The Q-branch frequencies of the E_{3s} component of ν_3 (cm^{-1})

J	K	calc.	obs.	obs-calc
0	0	994.794	994.795	0.000
1	0	994.782	994.781	-0.001
2*	2	994.769	994.769	0.001
2	0	994.757	994.754	-0.003
3*	2	994.731	994.731	0.000
3	0	994.720	994.723	0.003
4	4	994.717	994.716	-0.001
4	2	994.682	994.678	-0.003
4	0	994.670	994.667	-0.003
5	4	994.655	994.661	0.006
5	2	994.620	994.624	0.004
5	0	994.608	994.609	0.001
6	4	994.580	994.584	0.004
6*	2	994.545	994.546	0.001
6	0	994.533	994.538	0.004
7	4	994.493	994.497	0.003
7*	2	994.458	994.457	-0.001
7	0	994.446	994.445	-0.001
8	4	994.394	994.398	0.004
8	2	994.359	994.357	-0.001
8	0	994.347	994.348	0.001
9	4	994.282	994.285	0.003
9*	2	994.247	994.246	-0.001
9	0	994.235	994.236	0.001
10	4	994.158	994.160	0.002
10*	2	994.123	994.124	0.001
10	0	994.111	994.112	0.001
11	4	994.021	994.023	0.002
11*	2	993.986	993.986	-0.001
11	0	993.974	993.974	0.000
12*	2	993.837	993.837	0.000
12	0	993.825	993.825	0.000

Table II,8: The Q-branch frequencies of the A_{1s} component of ν_3 (cm^{-1})

J	K	calc.	obs.	obs-cal
0	0	994.686	994.685	-0.001
1	0	994.673	994.677	0.004
2	2	994.660	994.661	0.000
2	0	994.648	994.647	-0.002
3	2	994.623	994.623	0.000
3	0	994.611	994.609	-0.002
4	2	994.573	994.574	0.000
4	0	994.561	994.560	-0.001
5	2	994.511	994.513	0.002
5*	0	994.499	994.499	0.000
6	2	994.437	994.437	0.001
6*	0	994.425	994.424	-0.001
7	2	994.350	994.348	-0.001
7*	0	994.338	994.338	0.000
8	2	994.250	994.250	0.000
8	0	994.238	994.239	0.000
9	2	994.138	994.139	0.001
9	0	994.127	994.126	-0.001
10	2	994.014	994.013	-0.001
10	0	994.002	994.004	0.002
11	2	993.878	993.877	0.000
11	0	993.866	993.870	0.004
12	2	993.729	993.727	-0.001
12	0	993.717	993.717	0.000

Table II,9: The Q-branch frequencies of the E_{3d} component of ν_3 (cm^{-1})

J	K	calc.	obs.	obs-calc
1*	1	994.689	994.691	0.002
2*	1	994.664	994.666	0.001
3	3	994.651	994.648	-0.002
3*	1	994.627	994.625	-0.002
4	3	994.601	994.599	-0.001
4*	1	994.577	994.576	-0.002
5*	3	994.539	994.540	0.001
5	1	994.515	994.514	-0.001
6	3	994.464	994.464	0.000
6*	1	994.441	994.439	-0.001
7	3	994.377	994.377	0.000
7*	1	994.354	994.355	0.001
8	3	994.278	994.277	-0.001
8*	1	994.254	994.254	0.000
9	3	994.166	994.165	-0.001
9*	1	994.143	994.144	0.001
10	3	994.042	994.045	0.003
10*	1	994.018	994.020	0.002
11	3	993.905	993.908	0.003
11*	1	993.882	993.883	0.002

Table II,10: Vibrational-rotational Parameters for ν_3 (cm^{-1})

	A_{3d} ν_3	E_{3s} ν_3	E_{3d} ν_3	A_{1s} ν_3
	993.612(3)	994.794(3)	994.699(4)	994.685(4)
α_B	0.0062106(86)			
α_A	0.003274(51)			
A	2.670948(51)			
B	0.6568173(90)			

of table II,10 are the resultant values of α_B and α_A which were combined with the ground state rotational constants given in table II,4 to calculate the ν_3=1 state B and A values.

Spectral simulation

A key part of the spectral analysis was the generation of simulated spectra based on the predictions of Fermi resonance and the statistical weights. In the simulation process of the CARS jet spectra, various line broadening contributions were considered. The natural line width is negligible so that collisional, Doppler and instrumental effects will dominate. The instrumental line width is

known to be 0.005 cm^{-1} from similar previous studies. A Doppler line width of 0.0009 cm^{-1} was calculated from equation II,7 using a jet teperature of 50 K. This is the estimated rotational temperature corresponding to trace c of figure II,17, obtained by rotational temperature analysis of the strong lines in the A_{3d} band region. By empirical adjustment, different collisional line widths were tried and a collisional line width of about 0.003 cm^{-1} was found to reproduce the observed spectrum.

In the simulation processs, calculated transitions for each of the four torsional sublevel band were first obtained using equation II,9 and the parameters resulting from the fitting process given in table II,10. Each transition was then given a Lorentzian shape and both real and imaginary parts of the CARS χ were convoluted by a Gaussian Doppler profile. Finally, the different parts of χ were squared, added, and then convoluted by the laser line shape, also assumed to be Gaussian. The result of the simulation are shown in figure II,19 for the A_{3d} band.

For the other three sublevels the assignment and simulated spectra are shown in figure II,20. The sum spectrum was simulated for all three components combined to show the good agreement with the experimental scan. Shown below are the simulations of each component in order to make it easier for the reader to see the assignments and

the shape of each torsional subband. Finally, the spectrum was simulated for all four components combined together at room temperature. The result of the latter simulation is shown in figure II,21. The general good agreement between the observed and the calculated spectrum at room temperature strongly supports the way in which the spectrum has been analyzed although some differences are apparent. These undoubtedly came from higher K transitions and a more complete analysis of this room temperature data is underway in a collaberation with S. Montero and students in Madred.

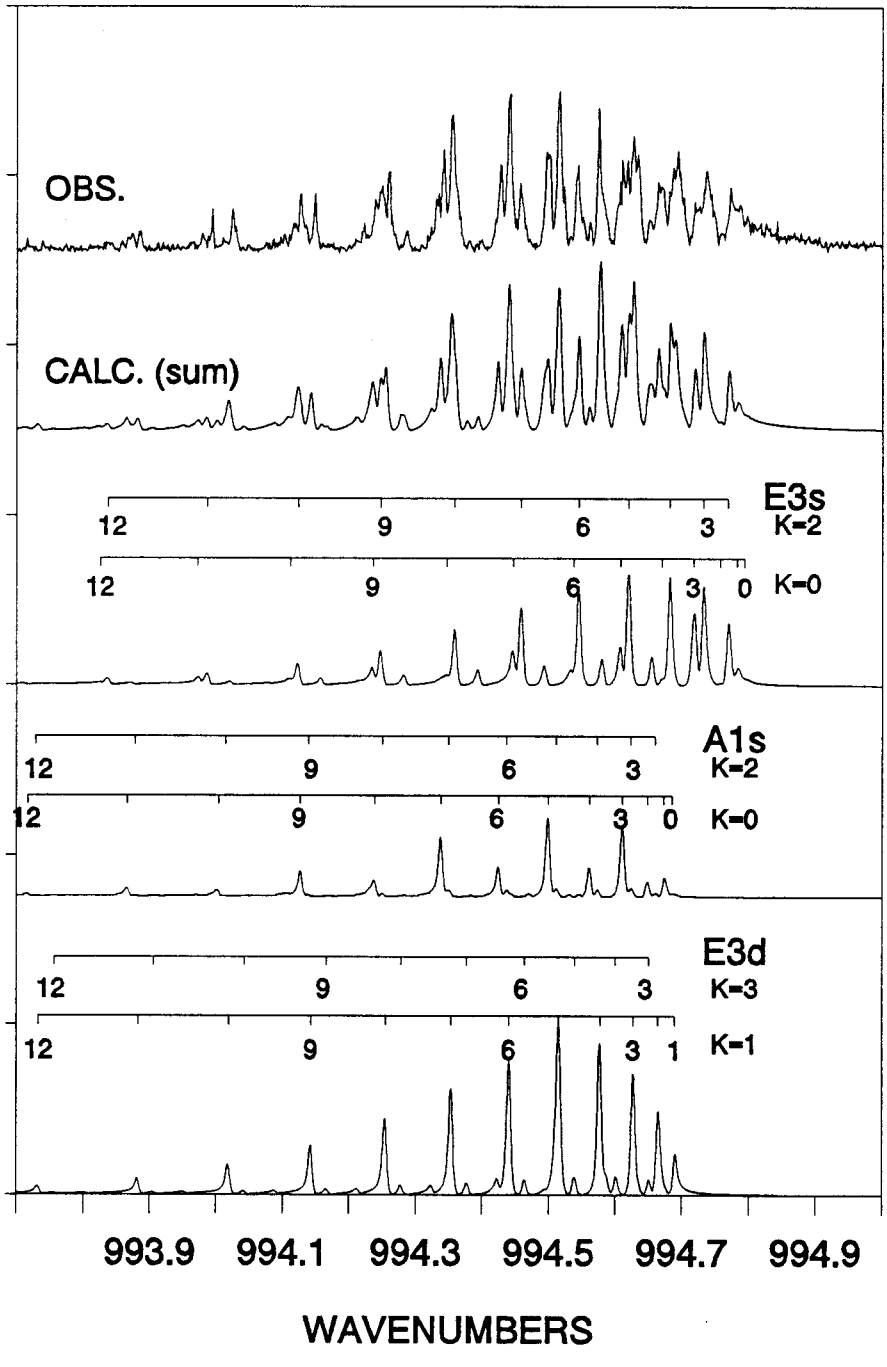

Figure II,20: Assignments and simulated spectra of E_{3s}, E_{3d}, and A_{1s} torsional sub levels of ν_3 at 50 K.

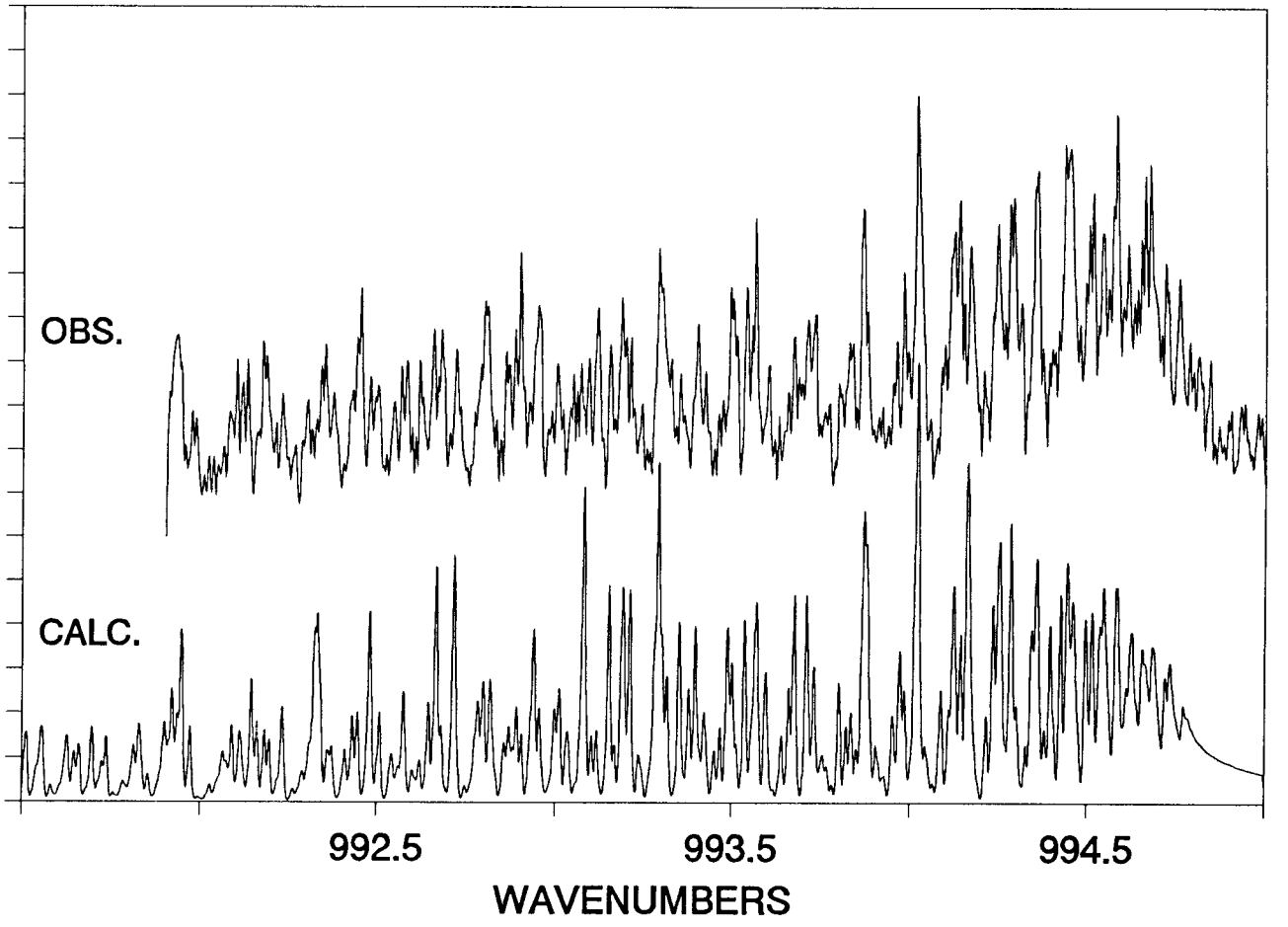

Figure II,21. Simulated spectrum of ν_3 at room temperature.

E: Summary and Discussion

This study has given the first high resolution data for the pure rotation of ethane and the ν_3 vibrational-rotational Q-branch. The full set of spectroscopic parameters resulting from both studies have been given in tables II,4, and II,10.

In the pure rotational Raman spectra, the measured transitions for S(10) to S(30) show no torsional splitting, confirming that such splittings are very small for the ground state and the first torsional excited state. The results shown in table II,4 show that when the torsional mode is excited by one quantum, the rotational constant B decreases by 0.00264 cm^{-1}. This small decrease indicates that the moment of inertia <u>increases</u> slightly on torsional excitation. This can be understood as resulting from increased repulsion of the two CH_3 rotors as the torsional amplitude increases toward the high parrier "eclipsed" form. This could manifest itself as either a slight C-C bond increase (0.003 Å) or as a decrease in the H-C-H angles (-0.5°) or, more likely, as a contribution of both. If the rotational constant A could be determined, the relative mix of these coordinate changes could be ascertained since A is independent of a C-C bond change. Unfortunately, A is unknown for the (υ_4=1) state so that

this partitioning of structural change can not be determined from our results.

Of particular interest is our observation of the Fermi resonance interaction of ν_3 with the $4\nu_4$ overtone. The clear spectral resolution of the ν_3 Q branch gives accurate results that are consistent with the existence of torsional sublevels of different symmetry. The successful analysis of the complix spectrum using the full G_{36}^+ group serves as an excellent example illustrating the use of double-group theory in an ethane-like molecule.

The interaction of ν_3 torsional sublevels with their counterparts of $4\nu_4$ is consistant with earlier predictions of the $4\nu_4$ torsional sublevels patterns based on a torsional barrier with V_3=1012 cm^{-1} and V_6=0 cm^{-1} [33]. The A_{1s} torsional sublevel of $4\nu_4$ has the greatest separation (-119.2 cm^{-1}) from the expected band origin of the ν_3 fundamental. This large separation will result in a very small Fermi resonance interaction shift for the A_{1s} sublevel of ν_3. Therefore, the band origin of A_{1s} sublevel of ν_3 at 994.685 cm^{-1} can be taken as a good approximation to the ν_3 band origin (994.685±0.2 cm^{-1}). This value is in much better accord with the low resolution estimate of 994.75 of Romanko et al[36] than with the value of 992.9 reported by Halvoort et al[33].

From the B values of the ground state and the ν_3 = 1

state given in tables II,4 and II,10, one can estimate that the C-C bond distance increases from 1.534 to 1.537 Å on vibrational excitation of this mode of the molecule.

As mentioned earlier the centrifugal distortion constants could not be determined from the spectra simplified of ethane in the jet. At the low temperatures of such expansions only energy levels with low K values are populated, resulting in poor values for all K dependent parameters. Further analysis using higher temperature scans such as room temperature scan would help in determining these parameters. Also, as a further study, the ν_3 band origin could be exactly tedermined by measuring one of the $4\nu_4$ sublevels. A_{3d} is a good candidate for such an investigation since it is closer to the ν_3 band origin and it would probably gain intensity due to the Fermi resonance interaction.

BIBLIOGRAPHY

1. A. Burg and H. I. Schlesinger, J. Amer. Chem. Soc.,62, 3425 (1940).

2. J. W. Nibler, J. Amer. Chem. Soc., 94, 3349, (1972).

3. D. S. Marynick and W. N. Lipscomp, J. Amer. Chem. Soc., 11, 820 (1972).

4. H. C. Longuet-Higgins and R. P. Bell, J. Amer. Chem. Soc., 250 (1943).

5. A. Almenningen, G. Gundersen and A. Haaland, Chem. commun.,557 (1967).

6. J. W. Nibler and T. Dyke, J. Amer. Chem. Soc., 92, 2920 (1970).

7. T. H. Cook and G. L. Morgan, J. Amer. Chem. Soc., 91, 774 (1969).

8. G. Gundesen, L. Hedberg and K. Hedberg, J. Chem. Phys., 59, 3777 (1973).

9. D. S. Marynick and W. N. Lipscomp, J. Amer. Chem. Soc., 95, 7244 (1973).

10. J. W. Nibler, D. F. Shriver and T. H. Cook, I. Chem. Phys., 54, 5257 (1971).

11. J. F. Stanton, W. N. Lipscomp and R. J. Bartlett, J. Chem. Phys., 88,5726 (1988).

12. I. N. Levine, "Molecular Spectroscopy", Wiley, New York (1975)

13. A. Weber, J. CHem. Phys., 73, 3952 (1980).

14. A. Weber, J. Chem. Phys., 76, 3694 (1982).

15. J. M. Hollas, " Modern Spectroscopy", Wiley, New York (1988).

16. G. D. Graybeal, "Molecular Spectroscopy", McGraw Hill, New York (1988).

17. G. Herzberg, "Molecular Spectra and Molecular Structure II: Infrared and Raman Spectra Of Polyatomic Molecules", Van Nostrand, Princeton (1945).

18. S. J. Daunt, W. E. Blass, G. W. Halsey, K. Fox, R. J. Lovell, H. Flicker and J. D. King, J. Mol. Spectry., 86, 307 (1981).

19. G. T. Forrest, Appl. Opt., 19, 2094 (1980).

20. K. F. Lin, W. E. Blass and N. M. Gailar, J. Mol. Spectry, 79. 151 (1980).

21. A. Cole, K. J. Cross, J. A. Cugley and H. M. Heise, J. Mol. Spectry, 83, 233 (1980).

22. C. W. Pattersen, H. Flicker, R. S. McDowell and N. G. Nereson, Mol. Phys., 43, 517 (1981).

23. R. J. Snyder, A. L. Aljibury, H. L. Strauss, H. L. Casal, K. M. Gough and W. M. Murphy, J. Chem. Phys., 81, 5352 (1984).

24. F. C. Baglin, U. Zimmerman and H. Versmold, Mol. Phys., 52, 877 (1984).

25. J. Martin and S. Montero, J. Chem. Phys., 80, 4610 (1984).

26. J. M. Fernandez-Sanches, A. D. Valdenebro and S. Montero, J. Chem. Phys., 91, 3327 (1989).

27. D. W. Lepard, D. E. Shaw and H. L. Welsh, Can. J. Phys., 44, 2353 (1966).

28. P. R. Bunker, Mol. Phys., 8, 81 (1964).

29. S. Weiss and G. E. Leroi, J. Chem. Phys., 48, 962 (1968).

30. J. T. Hougen, J. Mol. Spectry., 82, 92 (1980).

31. H. C. Longuet-Higgins, Mol. Phys., 6, 445 (1963).

32. N. Moazzen-Ahmadi, H. P. Gush, M. Halpern, H. Jagannath, A. Leung and I. Ozier, J. Chem. Phys., 88, 563 (1988).

33. K. Van Helvoort, W. Knippers, R. Fantoni and S. Stolte, Chem. Phys., 111, 445 (1987).

34. W. E. Blass, G. W. Halsey, J. Susskind, D. C. Reuter and D. E. Jennings, J. Mol. Spectry., 141, 334 (1990).

35. A. Weber, "The Raman Effect",vol. 2, ed. by A. Anderson, M. Dekker, New York (1973).

36. J. Romanko, T feldman and H. Welsh, Can. J. Phys., 33, 588 (1955).

37. K. Brown, PhD Dissertation, Oregon State University, (1991).

38. L. P. Guss, J. W. Fleming and A. B. Harvey, Opt. Soc. Amer., 5, 345 (1980)

39. J. W. Nibler and G. V. Knighten, "Raman Spectroscopy of Gases and Liquids", vol. 11, ed. by A. Weber, Springer- Verlag, Berlin and New York (1979).

40. G. A. Pubans, PhD dissertation, Oregon State University.

41. C. V. Raman and K. S. Krishnan, Nature, 121, 508 (1928).

42. J. W. Nibler and G. A. Pubanz, "Advances in Nonlinear Spectroscopy", vol. 15, ed. by R. Clark and R. Hester, Wiley, New York (1988).

43. A. Owyoung, G. R. Hadley, P. Esheric, R. L. Schmitt and L. A. Rahn, Opt. Lett. 10, 484(1985).